Atmospheric Environment 296 (2023) 119539

Contents lists available at ScienceDirect

Atmospheric Environment

journal homepage: www.elsevier.com/locate/atmosenv

On the Middle East's severe dust storms in spring 2022: Triggers and impacts

Diana Francis [a,*], Ricardo Fonseca [a], Narendra Nelli [a], Deniz Bozkurt [b], Juan Cuesta [c], Emmanuel Bosc [d]

[a] Environmental and Geophysical Sciences (ENGEOS) Lab, Earth Science Department, Khalifa University, P.O. Box 127788, Abu Dhabi, United Arab Emirates
[b] Department of Meteorology, Universidad de Valparaíso, 2340000, Valparaíso, Chile
[c] Univ Paris Est Créteil and Université Paris Cité, CNRS, LISA, F-94010, Créteil, France
[d] Federal Authority for Nuclear Regulation (FANR), P.O. Box: 112021, Abu Dhabi, United Arab Emirates

HIGHLIGHTS

- Cut-off lows over eastern Mediterranean fueled by tropical atmospheric rivers, led to widespread convection over Turkey and neighboring regions.
- Density currents emanating from convection triggered severe dust storms that significantly impacted the radiative budget and the boundary layer structure.
- A warming effect of the dust was observed over the southern Arabian Peninsula both at the ground and throughout the dust layer.

ARTICLE INFO

Keywords:
Dust storms
Density currents
Drylands
Cut-off low
Atmospheric rivers
IASI

ABSTRACT

Large amounts of dust in the air can disrupt daily activities and pose a threat to human health. In May 2022, consecutive major dust storms occurred over the Middle East resulting in severe environmental, social and health impacts. In this study, we investigate the exceptional factors driving these storms and the effects of the dust clouds. Using a combination of satellite, in-situ and reanalysis datasets, we identify the atmospheric triggers for the occurrence of these severe dust storms, characterize their three-dimensional structure and evaluate the dust radiative impact. The dust emission was promoted by density currents emanating from deep convection over Turkey. The convective systems were triggered by cut-off lows from mid-latitudes fed by moisture from African atmospheric rivers. Data from the Infrared Atmospheric Sounding Interferometer (IASI) showed that the dust clouds were transported southward at 4 km in altitudes but sunk to ground levels when they reached the southern Arabian Peninsula due to strong subsidence. At a station in coastal UAE, the dust caused a 350 W m^{-2} drop in the surface downward shortwave flux and a 70 W m^{-2} increase in the longwave one during the dust episodes. This contributed to a 9 °C increase in nighttime temperatures which exacerbated the effects of the heat for the population. The newly highlighted mechanism for dust emission in the Middle East, in which a cut-off low interacts with an atmospheric river, as well as direct observations of the dust impact on the radiative budget can contribute to reducing associated uncertainties in climate models.

1. Introduction

Aerosols, defined as solid or liquid particles suspended in the air, are an important component of the climate system (Li et al., 2022). In fact, aerosol radiative forcing, which offsets about a third of the warming caused by anthropogenic greenhouse gasses, is the largest source of uncertainty in climate change studies (IPCC et al., 2021). One of the most prevailing aerosol types is mineral dust, 90% of which originates from the North African and Asian deserts, and has important regional and global climate effects (Francis et al., 2021a; Kok et al., 2021; Zittis et al., 2022). Dust particles generally scatter the incoming sunlight and trap the longwave radiation emitted by the Earth's surface which perturbs the energy budget at the surface and top of the atmosphere (TOA, Slingo et al., 2006; Li et al., 2022). However, the net radiative effect of dust aerosols remains uncertain (IPCC et al., 2021) mainly because the reported radiative impacts are modulated by several factors. They

* Corresponding author.
E-mail address: diana.francis@ku.ac.ae (D. Francis).

https://doi.org/10.1016/j.atmosenv.2022.119539
Received 5 September 2022; Received in revised form 23 November 2022; Accepted 11 December 2022
Available online 23 December 2022

include: (i) the chemical composition of the dust particles, which impacts how they interact with the solar radiation (e.g. the East Asian dust is more absorptive of solar radiation than the Saharan dust; Huang et al., 2014); (ii) the vertical distribution of dust loading (e.g. Johnson et al., 2008); (iii) the proximity to the dust source region (e.g. Zhao et al., 2003); (iv) the nature of the surface below (e.g. if it is water or land; Francis et al., 2022a).

The expected expansion of arid regions in a warming world may lead to an increase in regional and global dust activity (Huang et al., 2020; Behzad et al., 2022). This is particularly true in the Middle East, where new dust source regions have arisen in the last couple of decades, in particular in Iraq, Syria, Jordan and Saudi Arabia, in the form of dry river beds (wadis) and lakes, providing additional sources of easily-erodible materials (Salmabadi et al., 2020). Besides the increasing desertification, droughts have become more frequent and intense in the Middle East in the recent decades, in particular in Iraq (Hameed et al., 2018) and Syria (Mathbout et al., 2018) where major dust sources are located. In fact, the two severe drought episodes in 2000–2001 and 2007–2012 led to a 52% drop in water bodies and a 14–37% increase in sand and dust storms emission in the Middle East compared to the pre-2020 period (Papi et al., 2022), mostly in Syria and Iraq and in parts of Iran and Turkey. As dust emitted here can be transported downstream over long distances by the prevailing winds (Francis et al., 2022b), it can impact regions much bigger than the dust emitting region itself. For instance, dust emitted in Syria and Iraq is transported southeastward by the background Shamal winds (northwesterly) affecting major cities such as Abu Dhabi, Dubai and Muscat (Gandham et al., 2020), and with a favorable large-scale circulation can be advected all the way to East Asia and the Pacific Ocean (Tanaka et al., 2005). Dust aerosols can also interact with clouds (indirect effect; Albrecht, 1989) and modify the atmospheric circulation via its interaction with radiation (direct and semi-direct effects; Li et al., 2022). The latter can, in turn, modify monsoon systems (Gu et al., 2016), tropical cyclones' activity (Rosenfeld et al., 2012) and the regional circulation (Li et al., 2011) especially at near source regions where the amount of dust in the atmosphere is still significant (Kok et al., 2021). However, these interactions and feedback between atmospheric dust and the climate remain poorly quantified (IPCC et al., 2021). Therefore, there is a need to assess the impact of dust aerosols near the source regions such as the Middle East so as to improve their representation in current and future climate studies. Besides its meteorological impacts, mineral dust has profound socio-economic effects (Kalenderski et al., 2013; Miri et al., 2009; Middleton, 2017; Beegum et al., 2018). For example, during a major dust storm in April 2015 in the Middle East there was an increase in hospital admissions, traffic accidents, airport delays and major disruptions to education, construction, leisure and energy activities (Middleton et al., 2021). Hence, a better understanding of the chain of processes during dust events will help in mitigating its societal impacts through more targeted and better designed policies (Middleton and Kang, 2017).

Dust emission can arise from mesoscale phenomena and synoptic-scale forcing which comprises cold pools from convective systems (Bou Karam et al., 2014; Solomos et al., 2017), downward momentum mixing from the nighttime low-level jet (Allen and Washington, 2014; Bou Karam Francis et al., 2017), land-sea breezes (Parajuli et al., 2020), cold fronts from the mid-latitudes (Kaskaoutis et al., 2019a), dry cyclones (Francis et al., 2019, 2021a) and persistent pressure gradients that give rise to a continuously strong low-level flow, as was the case in June 2020 over the Sahara (e.g. Francis et al., 2020a). Mohammadpour et al. (2022) investigated the weather regimes responsible for the extreme dust loadings observed in the Middle East and southwest Asia from 2003 to 2012. The authors identified four major modes: (i) Southeast Arabia, (ii) Arabian Sea; (iii) Thar Desert; (iv) Aden Gulf. In (i), dust accumulates over the southeastern Arabian Peninsula as a result of a downstream transport by the Shamal winds. An extreme event of this nature took place in March 2012, where the presence of a ridge over the Arabian Sea helped to transport the dust from the Arabian Peninsula into India where it had a major impact in air quality (Singh and Beegum, 2013; Singh et al., 2016; Namdari et al., 2018). In (ii), dust is trapped in the northern Arabian Sea due to the convergence of the Shamal winds from the northwest, the southwest monsoon flow and the Levar winds from Iran and Pakistan, as also noted by Rashki et al. (2019), with dust emission in the eastern Arabian Peninsula and in the Sistan basin in Pakistan. A particularly strong event took place in June 2008, when a westward shift and strengthening of the Indian summer monsoon low coupled with a dry Sistan basin and increased dust emission, led to a spatially-averaged monthly AOD over the Arabian Sea higher than the 2000–2013 June climatology by 0.5 or ~78% (Kaskaoutis et al., 2014). In (iii), dust emission over the Thar Desert, located along the India-Pakistan border, is triggered by a deeper thermal low and associated stronger surface winds, while in (iv), dust lifting is triggered by the northwesterly flow associated with a ridge over north Africa and the Arabian heat low, with the dust trapped in the Gulf of Aden by a weaker southwest monsoon flow. These four weather regimes prevail in the warmer months, with wintertime dust lifting typically associated with the passage of cold fronts, some of which can carry Saharan dust into the Arabian Peninsula (Notaro et al., 2013; Hamzeh et al., 2021), and can be accompanied by a cut-off low in the mid- and upper-troposphere, as was the case in the February 2019 dust event in the Sistan Basin (Kaskaoutis et al., 2019b). Such cold season dust lifting occurrences explain the secondary maximum in dust loading in the southeastern Arabian Peninsula in February (Nelli et al., 2021). The fact that tropical and extratropical processes are involved in the dust emission in the region explains the different timing in the peaks of dust AOD in different parts of the Middle East (Rezazadeh et al., 2013). For example, in Iran the dust loading peaks can occur from March to November depending on the region (Mohammadpour et al., 2021). In the Arabian Peninsula and eastern Middle East, on the other hand, the highest dust loadings are observed in the summer months (Nelli et al., 2021).

Despite being one of the largest dust source regions in the world, the scarcity of ground-based observations has prevented the scientific community from a complete understanding of the mechanisms involved in dust emission in this region. Also, the dust properties and their radiative effects are still poorly understood in this region (e.g., Nelli et al., 2020; Zittis et al., 2022), as are its socio-economic impacts (Middleton et al., 2021). The field campaigns of Filioglou et al. (2020) and Kesti et al. (2022) revealed that the size plays a larger role than chemistry in the aerosol particle activation in the United Arab Emirates (UAE), with the Middle East dust properties generally comparable to those of the African dust. The numerical simulations of Fonseca et al. (2021) revealed that the aerosol loading and optical properties have an important impact on the warm season circulation in the Arabian Peninsula in particular on the thermal low, with small perturbations to both leading to big changes in the spatial distribution and intensity of the precipitation in the region.

In May 2022, exceptional dust storms in terms of their intensity and duration battered the Middle East and resulted in serious effects on the populations, such as health problems, due to worsening air quality over several days. Fig. 1 shows two intense dust storms over Iraq; the first one occurred on 16 May and the second on 23 May. The dust fronts are seen to propagate downstream into the southeastern Arabian Peninsula on the days following initial emission (17 and 24 May, respectively). In this work, the triggers and impacts of two May 2022 severe dust storms in the Middle East are investigated with reanalysis, satellite-derived and in-situ data. The mechanisms behind the dust lifting in Iraq, and why it occurred twice in one week in the same region are highlighted. Additionally, we take advantage of unique observational measurements in the UAE during the two dust events to gain further insight into the vertical distribution of dust aerosols and their radiative forcing.

This paper is structured as follows. Details regarding the observational and reanalysis datasets and the methodology considered in this study are given in section 2. The synoptic-scale circulation patterns that favored the dust events are identified in section 3. In section 4, we

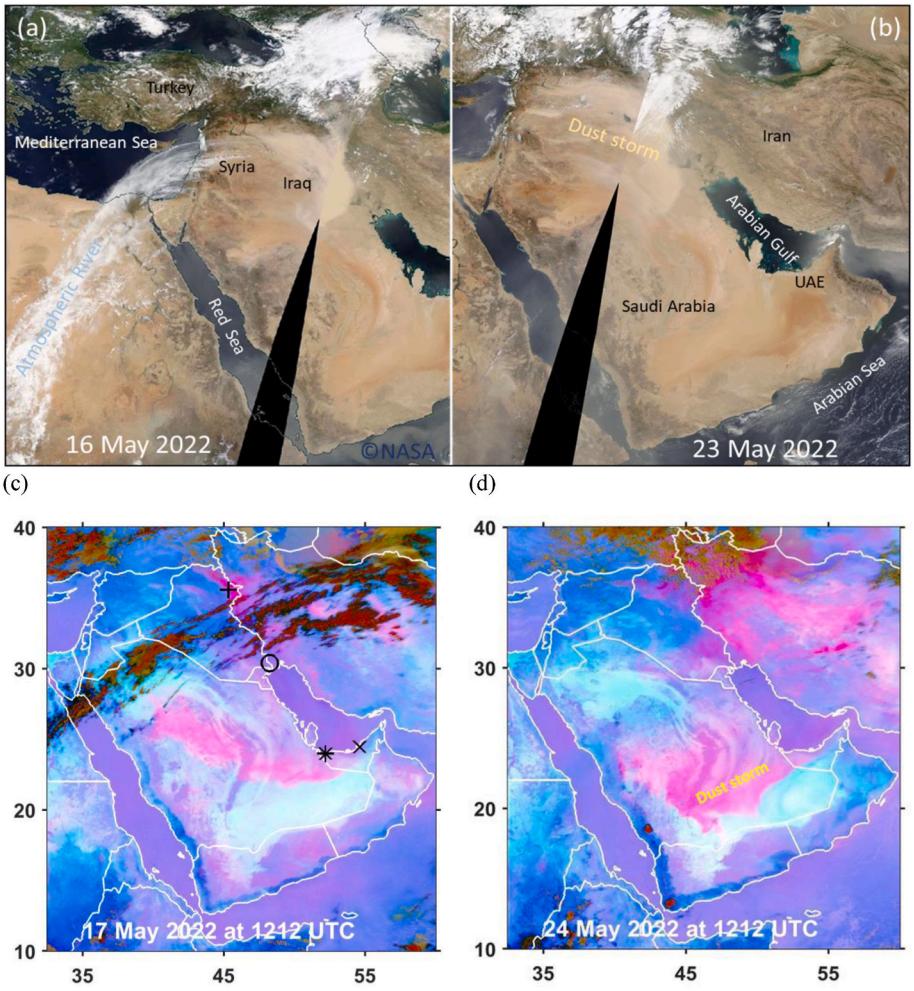

Fig. 1. The May 2022 dust storms: MODIS visible satellite imagery on (a) 16 and (b) May 23, 2022 showing dust emissions. Clouds are in white, land is given in dark brown, water bodies are represented in dark blue, and the light brown shading denotes dust plumes. Image credits NASA Worldview. SEVIRI false-colour images at 1212 UTC on (c) 17 and (d) May 24, 2022 showing dust transport. In these brightness temperature images, clouds appear in orange or brown, dust in magenta or pink, sandy regions in white, and dry land in pale blue. The asterisk, cross, circle and plus signs in panel (c) highlight the location of Barakah (52.21°E, 23.96°N) and Masdar City in Abu Dhabi (54.62°E, 24.44°N) in the UAE, the Abadan Ayatollah Jami International Airport (48.25°E, 30.37°N) in southwestern Iran and the Sulaimaniyah International Airport in northeastern Iraq (Meteorological Terminal Air Report Code: OSRU, 45.45°E, 35.53°N), respectively.

discuss the atmospheric triggers of the dust storms and analyze their spatio-temporal characterization. In section 5, the radiative impact of dust plumes is assessed. The main conclusions are summarized in section 6.

2. Observational and reanalysis datasets

A combination of ten observational and one reanalysis datasets are used in this study. Five satellite-derived products are considered. Dust plumes are identified using satellite images, both visible from the Moderate Resolution Spectral Radiometer (MODIS; Kaufman et al., 1997; Kaufman et al., 2002) instrument onboard the National Aeronautic and Space Administration's (NASA's) Terra and Aqua satellites, and false colour from the Spinning Enhanced Visible and Infrared Imager (SEVIRI; Schmetz et al., 2002; Banks et al., 2019) instrument onboard the Meteosat Second Generation spacecraft. MODIS images are available daily on NASA's Worldview application (Boller, 2022). SEVIRI's brightness temperature measurements at 8.7, 10.8 and 12 μm, available on a 0.05° grid every 15-min, are processed to generate false colour images where dust plumes can be easily identified following Martinez et al. (2009). AOD from MODIS, available daily at a 1° spatial resolution, is used to quantify the amount of lofted dust in the region. Dust loading and its vertical distribution are also extracted from the AEROIASI product. This data is obtained by combining meteorological inputs from the Infrared Atmospheric Sounding Interferometer (IASI) instrument onboard the European Organization for the Exploitation of Meteorological Satellites MetOp satellite, with an aerosol model as detailed in Cuesta et al. (2015). Surface and top of atmosphere radiative fluxes, estimated from satellite data and at 1° spatial and hourly temporal resolution, are available in the Clouds and the Earth's Radiant Energy System (CERES; Wielicki et al., 1996) dataset. Satellite-derived infrared brightness temperature, available every 30 min on a 4 km grid, are used to check for the presence of clouds, with a threshold value of 280 K used as per Reddy and Rao (2018).

Five in-situ measurement datasets are analyzed in this work. Hourly air temperature, wind direction, speed, and horizontal visibility at the Sulaimaniyah International Airport in northeastern Iraq (plus sign in Fig. 1c) and at the Abadan Ayatollah Jami International Airport in southwestern Iran (circle in Fig. 1c) are extracted from Meteorological Aerodrome Reports (METAR) data (Leslie and Jones-Bateman, 2022) to quantify the effects of dust on the near-surface environment and investigate the duration of dust episodes for two sites adjacent to the source region. Sounding temperature profiles, as measured by radiosondes launched twice daily at Abu Dhabi's International Airport (Oolman, 2022) are used to explore the dust impact on the tropospheric temperature. A Vaisala ceilometer, CL61, installed at Masdar Institute Solar Platform, Abu Dhabi (cross in Fig. 1c), was used to quantify the vertical extent of the dust storm in the present study. CL61 is a high-performance Light Detection and Ranging (LiDAR) instrument with depolarization measurement capable of unattended operation in all conditions. In addition to basic ceilometer reporting, the CL61 offers depolarization measurement that enables accurate liquid and frozen differentiation as well as detection of dust and volcanic ash layers. The raw CL61 range-corrected back scattered profiles are available at 36-s temporal resolution and 4.8-m vertical resolution. Besides detecting clouds, ceilometers are also useful for detecting aerosol layers at lower altitudes

(Munkel et al., 2007; Wiegner and Coauthors, 2014; Jin et al., 2015; Marcos et al., 2018; Yang et al., 2020; Evan et al., 2022). The Fernald-method (Fernald, 1984) is used to retrieve the aerosol extinction coefficient profile from backscattered signals. The dust impact on surface radiation fluxes was quantified utilizing netradiometer (Kipp and Zonen, 2022) measurements from a micrometeorological tower located at Barakah (asterisk in Fig. 1c; Nelli et al., 2022). In situ observations are also taken at Barakah by a portable weather station (Weston et al., 2022; Nelli et al., 2022). It measures 2-m temperature, relative humidity and 10-m wind speed and direction data every 60 s by a Lufft WS501-UMB (Weather Sensor 501 - Universal Measurement Bus system) smart weather sensor (Lufft, 2022).

Large-scale meteorological fields are extracted from the ERA-5 reanalysis data (Hersbach et al., 2020), available on an hourly basis and on a 0.25° grid from 1950 to present. ERA-5 data shows general good agreement with in situ observations in the Middle East (e.g. Fonseca et al., 2022), and its high spatial and temporal resolution allows for a detailed investigation of the mechanisms that triggered the dust event.

3. Synoptic-scale conditions

The synoptic-scale conditions for the period 14–24 May 2022 during which the two dust storms occurred are investigated using ERA-5 data. Fig. 2a shows the 300 hPa geopotential height and wind vector anomalies for the period of interest. The atmospheric circulation over the northern hemisphere was dominated by a wavenumber 5 pattern (Fig. 2a) with a pronounced blocking high over northwestern Europe, whose anomalies are more than two standard deviations above the 1979–2021 May climatology, and deep troughs over North Africa and western Russia. The slantwise omega blocking is seen in the wind vector

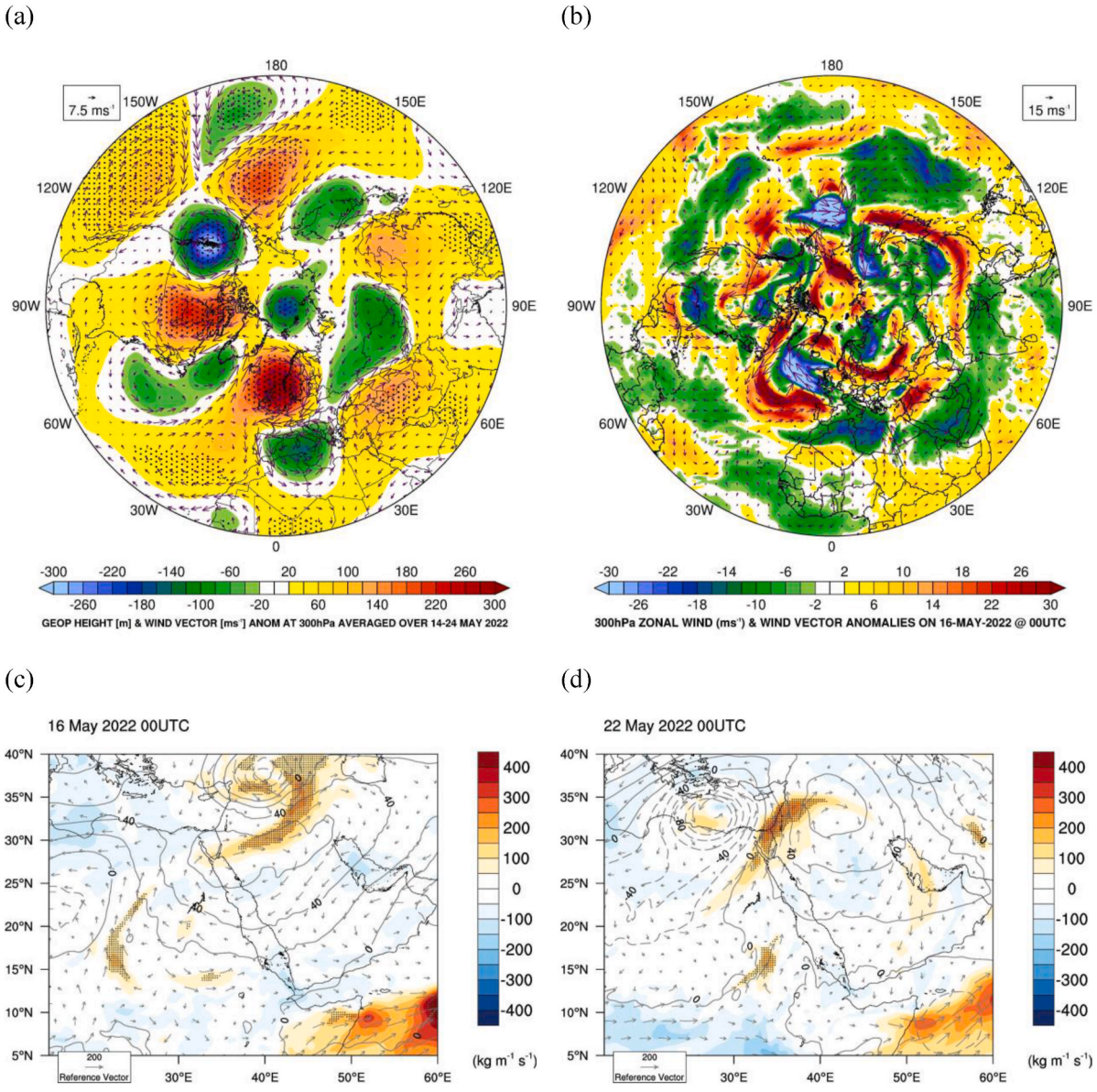

Fig. 2. Synoptic atmospheric circulation: (a) 300 hPa geopotential height (shading; m) and wind vectors (arrows; m s^{-1}) averaged over 14–24 May 2022. Regions where the anomalies are more than one standard deviation away from the 1979–2021 May climatology are stippled. (b) 300 hPa zonal wind speed (shading; m) and wind vector (arrows) anomalies, with respect to ERA-5's 1979–2021 climatology, on May 16, 2022 at 00 UTC. (c) Integrated Vapour Transport (IVT; kg m^{-1} s^{-1}) (the shading gives the magnitude and the arrows give the vectors) and 500 hPa geopotential height anomalies (black contours; m) on (c) 16 May and (d) May 22, 2022 at 00 UTC with respect to May climatology between 1979 and 2021. Hatching in the IVT fields corresponds to grids where the anomaly is greater than two standard deviations. The IVT fields were obtained from ERA5 by vertically integrating the 3-hr specific humidity and zonal and meridional winds for the whole air column extending from the surface to the top of the atmosphere.

anomaly (Fig. 2b), which also shows the poleward shift of the subtropical jet over the Arabian Peninsula and the southward shift of the polar jet over western Russia and the northern Atlantic Ocean. As a result of the pronounced equatorward displacement of the polar jet, a cut-off low was conceived over the eastern Mediterranean on 14 May (Figs. S1a-b) and was associated with a cold mid-to upper-troposphere (Fig. S1e). It migrated over Turkey on 15–16 May (Fig. 2c and S1c) and joined the low over Russia on 17 May. Cut-off lows, also known as cold drops (e.g., Francis et al., 2019), are closed upper-level lows that become detached from the mid-latitude westerly jet. They are associated with severe weather conditions due to an unstable vertical stratification, amplified by the daytime surface heating which fosters convection (Griffiths et al., 1998; Nieto et al., 2005). Cut-off lows in the warmer months over the Mediterranean region peak in June with a lifetime generally less than 36 h (Porcu et al., 2007). They are known to trigger severe flood over Europe (e.g., Zittis et al., 2022). Here, they are found to trigger severe dust storms over the Middle East as it will be demonstrated in section 4.

The blocking ridge over northern Middle East and Caspian Basin facilitated westerly/southwesterly flow along the eastern flank of the cut-off low. Fig. 2c and d shows an anomalous narrow band of moisture from tropical Africa, known as atmospheric river (AR, Massoud et al., 2020; Dezfuli et al., 2021; Bozkurt et al., 2021), being advected into the Middle East along the eastern flank of the cut-off lows. This significant supply of moisture via the AR helps in fueling the cut-off low and maintaining it over time (e.g., Francis et al., 2020b). As the cut-off low reached the mountainous regions over southeastern Turkey, deep convection developed (Figs. 1a and 3a) and generated convective-downdrafts and density currents over northern Iraq and Syria (Fig. 3a).

A similar set-up took place from 19 to 23 May (Fig. 2d and S1d), with another episode combining a cut-off low, an atmospheric river and convection, resulting in a second dust storm over the Middle East (Fig. 1b and d). In fact, the two synoptic-scale cut-off lows and atmospheric rivers that triggered convection and subsequent dusty density currents, developed from the same background large-scale pattern that was present during the period 14–24 May 2022. Toward the end of May's episodes, the trough over northern Africa weakened and a strong ridge moved into the eastern Mediterranean pushing the low over western Russia further east on 25 May, bringing the favorable synoptic-scale pattern for dust emission to an end.

4. Atmospheric triggers and dust storm characteristics

Turbulence and high surface-winds resulting from the convective-downdrafts and associated density currents (Fig. 3b and c) generated intense dust emission over several days (Fig. 3a) which later propagated downstream (Fig. 1c and d). The first dust emission occurred at 09 UTC on 15 May over central and southern portions of Syria, and dust continued to be emitted throughout the day (Fig. 3a). It reached its peak in the local evening hours when a convective system developed over Turkey. The associated downdrafts triggered density currents (e.g., Bou Karam et al., 2014) that propagated downstream into western and central Iraq and later into the southern parts of the Arabian Peninsula (Fig. 1c). The density currents are seen in Fig. 3b and c over central Iraq

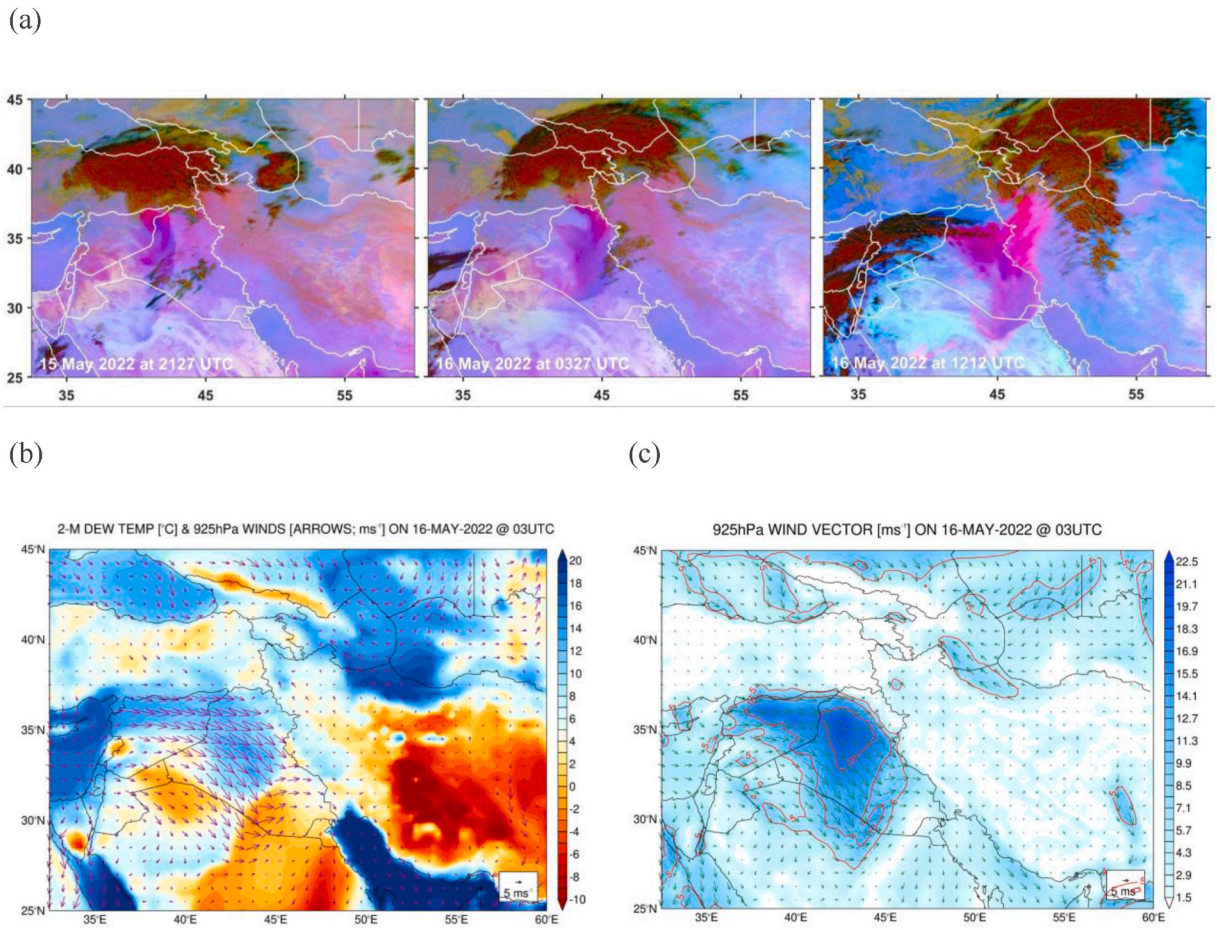

Fig. 3. Atmospheric dynamics causing dust emissions in first episode (15–16 May): (a) SEVIRI false colour satellite image on May 15, 2022 at about 21 UTC and 16 May at roughly 03 and 12 UTC. The conventions are as in Fig. 1c and d. (b) 2-m dewpoint temperature (shading; °C) and 925 hPa winds (arrows; m s^{-1}) on May 16, 2022 at 00 UTC. (c) Is as (b) but showing the 925 hPa vectors (arrows) and magnitude (shading; m s^{-1}). The red solid contours denote regions where the wind speed anomalies exceed the 1979–2021 May climatological values by 5, 10 and 15 m s^{-1}.

and are characterized by moist (note the jump of more than 10 °C in the 2-m dewpoint temperature) and dusty (pink shading in Fig. 3a) air, and accompanied by wind speeds in excess of 20 m s^{-1} (i.e., more than 15 m s^{-1} above the climatological values). For dust emission to occur over the Middle east, near-surface wind speeds higher than 7 m s^{-1} are needed (Yu et al., 2016), a value within the wind speed thresholds estimated for other arid regions such as the 4–12.5 m s^{-1} range for western Sahara (Helgren and Prospero, 1987). Dusty density currents emanating from deep convection and the associated dust emission are a regular occurrence in the tropics and subtropics during the monsoon season (e.g., Flamant et al., 2007; Bou Karam et al., 2008; Knippertz et al., 2007; Francis et al., 2021b) but they have not been reported in the Middle East and even less during the spring season.

A closer inspection of the 15 min SEVIRI satellite images revealed that the dust front propagated at speeds of up to 10 m s^{-1}, in line with the literature values for dusty density currents (e.g. Knippertz et al., 2007; Solomos et al., 2012). The large amounts of dust lifted by turbulent winds within the density currents can be explained by the fact that these fronts propagated over a newly formed dust source in Iraq; the Sawa Lake in the southern province of Muthanna which has completely dried up in 2022 for the first time in Iraq's history due to severe drought. Dry lake beds, such as the Bodele Depression in North Africa (Todd et al., 2008), are known to offer a copious source for dust emission since they are covered by fine particles and erodible materials that can be easily lifted by strong winds (Schepanski et al., 2007).

The presence of the cut-off low, fueled by moisture supplied by successive atmospheric rivers, helped to trigger and sustain the convection and therefore the dust emission. Worth mentioning the marked contrast between the very moist air over the Arabian Gulf, with 2-m dewpoint temperatures in excess of 25 °C, and the bone-dry air over Iran and Saudi Arabia, where the dewpoint temperatures drop below −10 °C (Fig. 3b) which is one of the unique features of the region (Fonseca et al., 2022).

The effects of the dust on the state of the atmosphere over the source area can be seen in Fig. 4a for an airport station in northeastern Iraq near the border with Iran (plus sign in Fig. 1c): on 16 May the visibility dropped to 150 m and the daily maximum temperature was 5 °C lower than on the previous day when the sky was clear (Fig. S2a), as dust acts to scatter the incoming solar radiation and hence cool the surface during the day (Todd et al., 2013; Weston et al., 2020). The arrival of the density current, at ~02:30 UTC or 05:30 local time (LT), on 16 May, is accompanied by a 5 °C jump in air temperature and a doubling of the wind speed, reaching a value roughly 10 °C above the May climatology. The second dust event, on 23–24 May, is of comparable magnitude, with a maximum temperature drop of 7 °C and a visibility that reached 350 m. The wind speed peaked just before the arrival of the dust plumes, reaching around 10 m s^{-1} on 23 May, an anomaly of about 4 m s^{-1} with respect to the background value. The density current over Iraq on 23 May is more zonally oriented than that on 16 May (cf. Figs. 4a and 3a), although it also led to substantial dust emission and subsequent downstream propagation in the region.

Long range transport of dust was aided by wind speeds in excess of 20 m s^{-1} over the Arabian Gulf extending into the UAE, Saudi Arabia and the borders of Oman and Yemen (Fig. 4d), corresponding to the nighttime low-level jet which formed in response to the dipole in pressure between the ridge in Saudi Arabia and the trough over Iran/Pakistan (Fig. 2c). Moisture advection from the Mediterranean Sea into the Arabian Gulf also took place during this event (Fig. 4c).

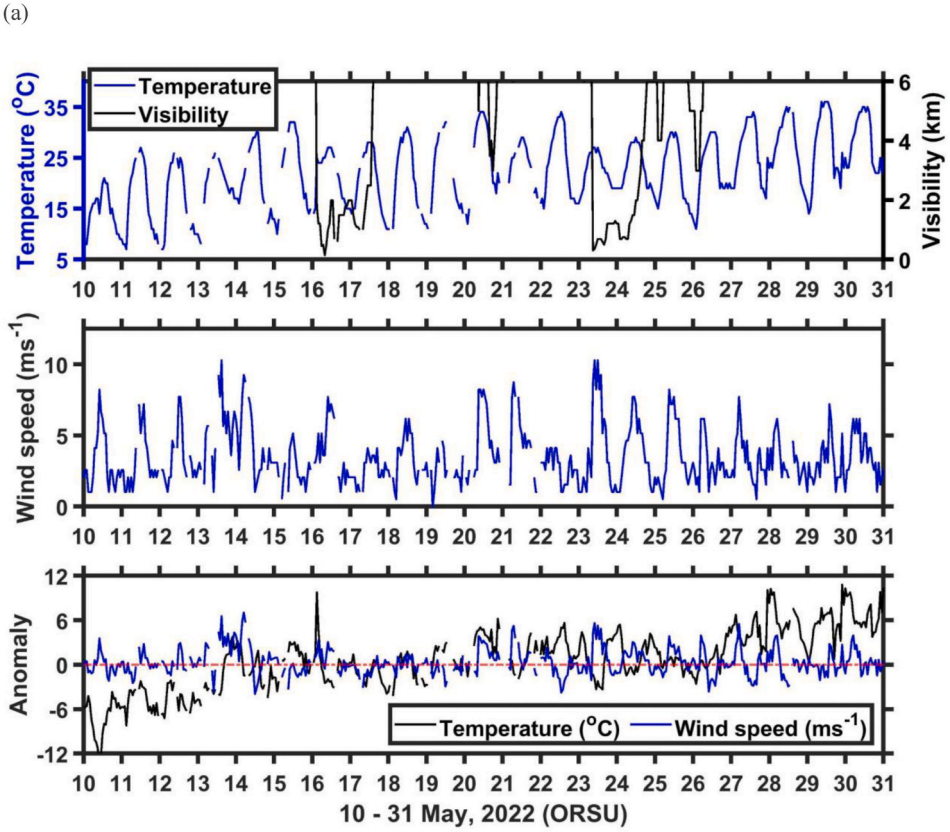

Fig. 4. Atmospheric dynamics causing dust emissions in second episode (23–24 May): (a) Air temperature (blue; °C) and visibility (black; km) in the top plot and wind speed (m s^{-1}) in the bottom plot from 10 to May 31, 2022 at the Sulaimaniyah International Airport (OSRU) in northeastern Iraq (plus sign in Fig. 1c). The bottom panel gives the anomalies with respect to the 2012–2019 May climatology. (b)–(d) are as Fig. 3a–c but for the May 24, 2022 dust event. In (b), the SEVIRI images are shown at roughly 18 UTC on 23 May and 00 and 06 UTC on 24 May, while the 2-m dewpoint temperature and winds in (c) and (d) are given at 00 UTC on May 24, 2022.

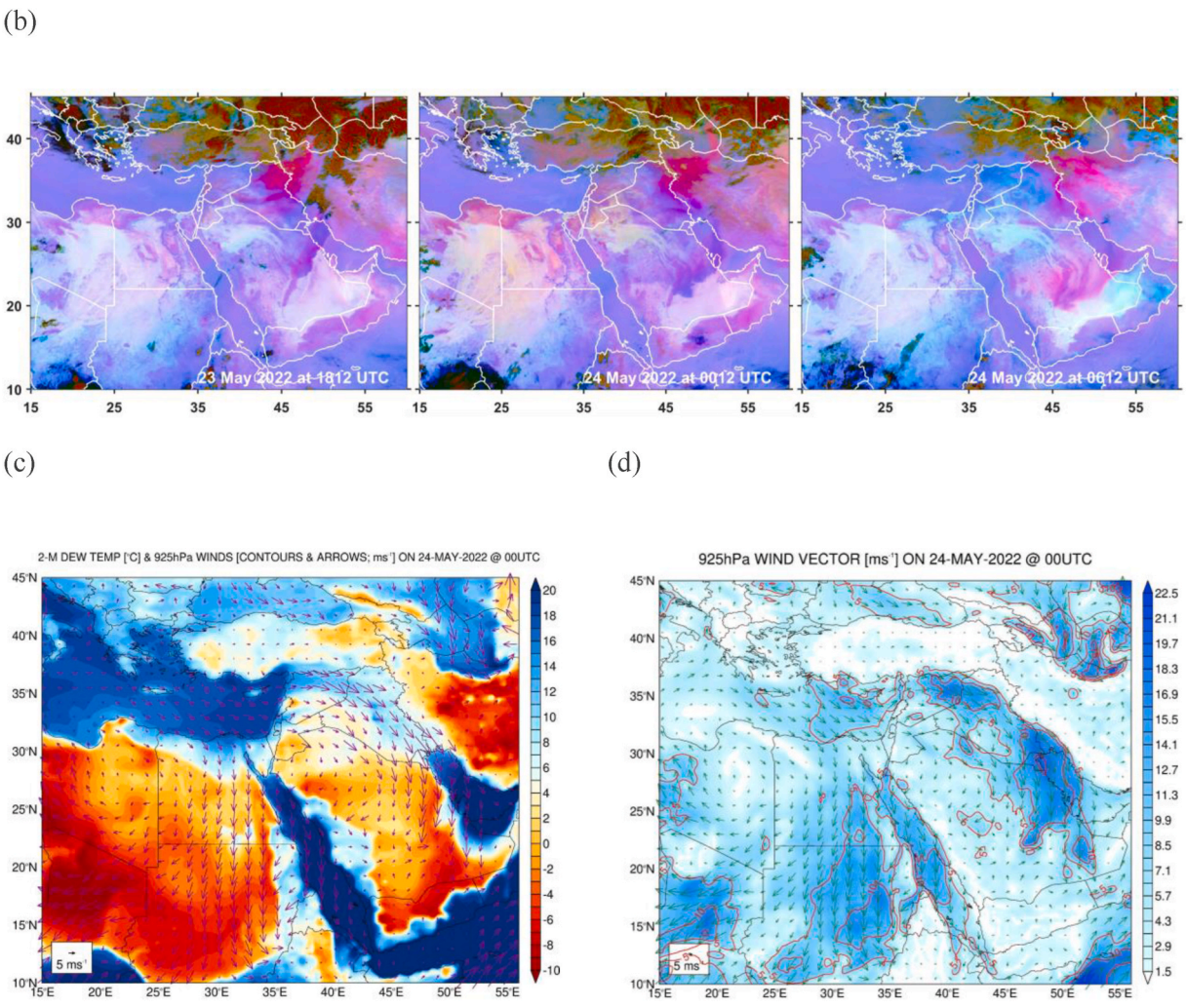

Fig. 4. (*continued*).

After emission in Syria and Iraq on 16 May, the dust propagated downstream into central and southern parts of the Arabian Peninsula following the counter-clockwise circulation associated with a ridge over the northern Red Sea (Fig. 5a) with the southeastward advection of the dust plumes favored by the background northwesterly winds (e.g., Francis et al., 2022b). This circulation also advects the more moist tropical air from Africa into Iran and the Arabian Gulf. In fact, the presence of an atmospheric river likely aids in the transport of dust, as noted by Dezfuli et al. (2021). AODs in excess of 2.5 were observed by the MODIS instrument, with the measurements interpolated to a $1^\circ \times 1^\circ$ grid and available daily, over western UAE and adjacent Saudi Arabia on 17 May (Fig. 5b) where the advancing dust front was located (Fig. 1c). AODs at 10 μm derived from the AEROIASI product (Cuesta et al., 2015, 2020), which provides vertical profiles of dust extinction coefficient derived from the Infrared Atmospheric Sounding Interferometer (IASI) instrument onboard the European Space Agency's MetOp polar orbiting satellites, were in excess of 0.8 on May 24, 2022 (Fig. 5c; no data is available on 17 and 23 May).

The dust layers were concentrated between roughly 1 and 5 km above ground level with a mean height around 4 km over the northern part of the Arabian Peninsula, decreasing gradually as the dust moved southern to be confined only below 1 km over the UAE and the Empty Quarter desert (Fig. 5d and e). This decrease in altitude as the dust plumes moved southward is due to the subsidence and air sinking associated with intense high pressure that was present over the central and southern part of the Arabian Peninsula during this time (Fig. 2d). This highlights the fact that despite being lifted far away, the dust can be brought to ground levels in some regions aided by subsidence, air compression and associated circulation. The 3D distribution of aerosol extinction at 10 μm from the AEROIASI satellite product indicates a thick layer near the ground over the UAE and southern Saudi Arabia, with less optically dense layers over the northern part of the Arabian Peninsula at 4 km in altitude (Fig. 5d).

Fig. 5f and g shows the observations by a ceilometer at Abu Dhabi on May 24, 2022. Several layers of dust aerosols are seen. The first layer near the ground is the thickest one, and is limiting the capability of the light signal to pass through. It extends up to ~600 m, with the associated inversion at the top seen in radiosonde profiles at the nearby airport (Fig. S3). Other stratified layers are present in the upper levels and exhibit undulatory structures over time. From AEROIASI and radiosonde (Fig. S3) observations, the top of the residual boundary layer for the same day was around 4.5 km and therefore consistent with the height of the boundary layer in a desert site (Cuesta et al., 2008; Nelli et al., 2021). High depolarization ratios near the surface around 0600 UTC and after 1000 UTC indicate the presence of large particles in the observed dust layers freshly emitted from the dust source. Throughout the day new thick dust layers were passing over the site and were sampled by the ceilometer. Low depolarization values were associated with dust transported over the site from long distances.

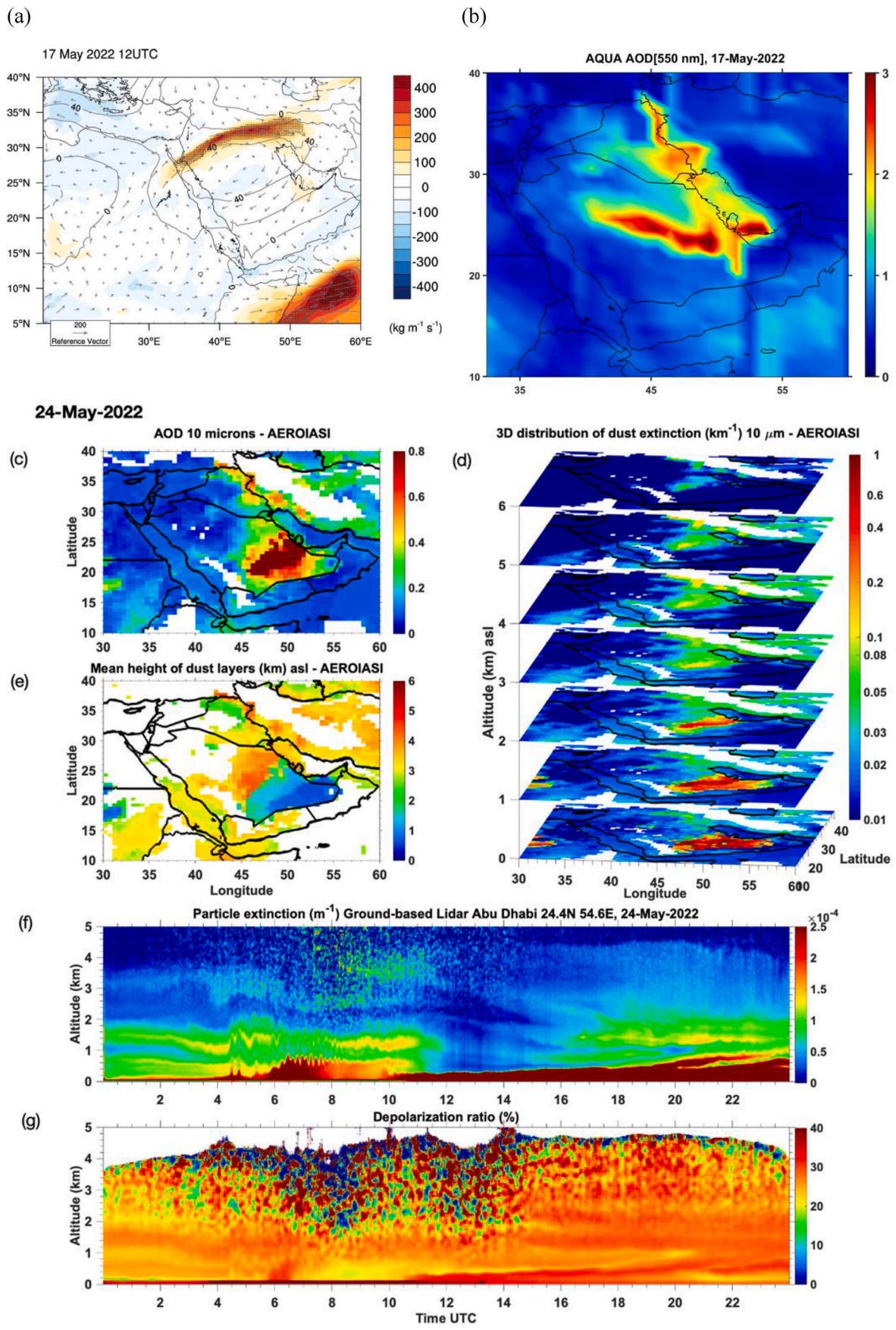

(caption on next page)

Fig. 5. Dust long-range transport: (a) IVT (the shading gives the magnitude and the arrows give the vectors; kg m^{-1} s^{-1}) and 500 hPa geopotential height (black contours; m) anomalies on May 17, 2022 at 12 UTC with respect to May climatology between 1979 and 2021. Hatching in the IVT fields corresponds to grids where the anomaly is greater than two standard deviations away from the mean. IVT fields were obtained from ERA5 by vertically integrating the 3-hr specific humidity and zonal and meridional winds for the whole air column extending from the surface to the top of the atmosphere. (b) Aerosol optical depth (AOD) at 550 nm and at 1° × 1° spatial resolution from the MODIS instrument on board the Aqua satellite on May 17, 2022. (c)–(e) AEROIASI products on May 24, 2022 at 0500 UTC. (c) AOD at 10 μm (d) vertical distribution of aerosol extinction and (e) mean height of the dust layers. (f) Particle extinction (m^{-1}) and (g) depolarization ratio (%) on May 24, 2022 from a ceilometer (CL61, Vaisala) located at Abu Dhabi (cross in Fig. 1c).

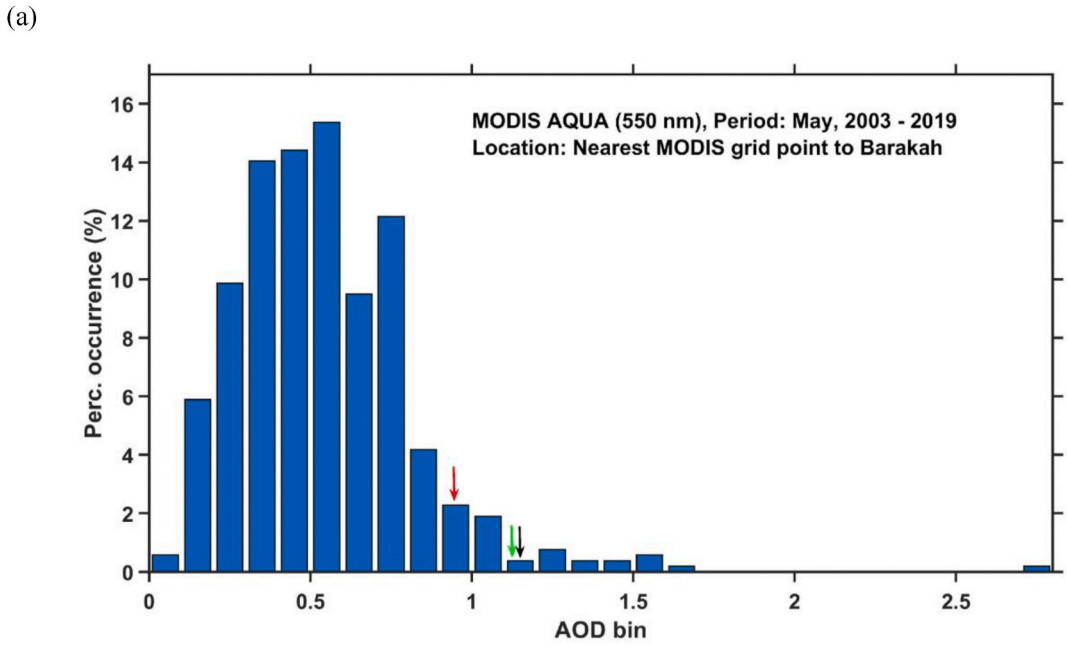

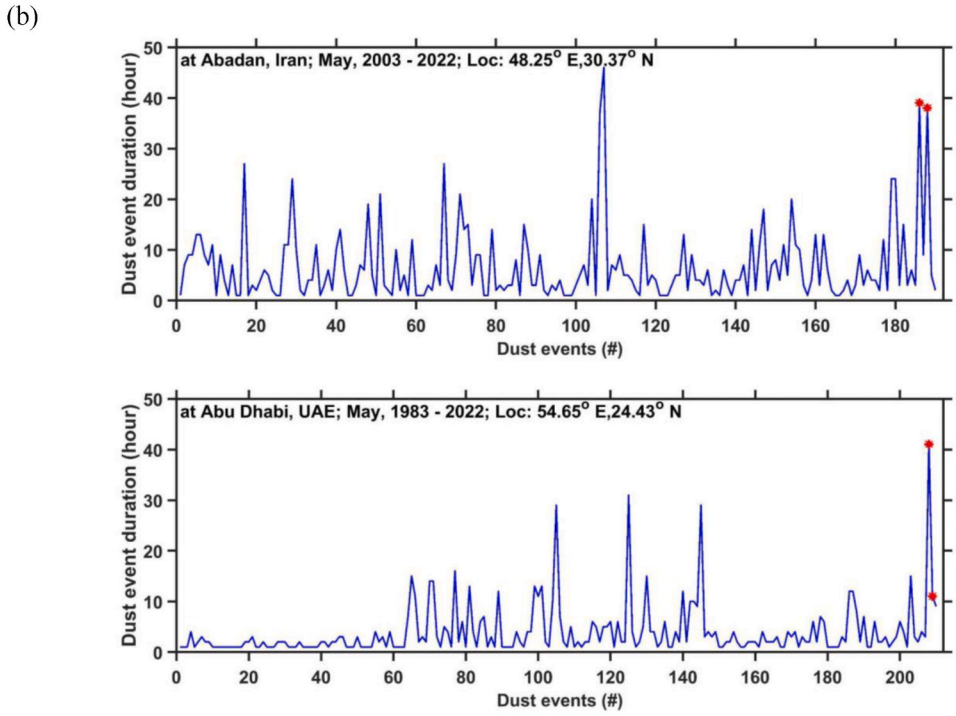

Fig. 6. Extreme nature of the dust storms: (a) Histogram of the AOD measured by the MODIS instrument on board the Aqua satellite at the closest grid-point to Barakah (blue; asterisk in Fig. 1c) for May 2003–2019. The red, black and green arrows give the AOD observed on 17, 19 and May 25, 2022, respectively. (b) Duration (hours) of all dust events at Abadan in southwestern Iran (circle in Fig. 1c), a site adjacent to the emission source, for all May days from 2003 to 2022 (top), and at Abu Dhabi in the UAE (cross in Fig. 1c), located downstream, for all May days in 1983–2022 (bottom). The red asterisks indicate the values on 17 and May 24, 2022.

5. Dust radiative impact

In this section, the radiative impacts of the dust events are assessed using in-situ measurements collected at Barakah in western UAE (asterisk in Fig. 1c) and satellite-derived radiative fluxes for the wider domain. The results are shown in Figs. 6 and 7.

At Barakah, the surface downward shortwave radiation flux dropped by roughly a third of its clear-sky value (~350 W m^{-2}) on 16–17 and 23–24 May when the dust plume was over the site (Fig. 1c and d, 7a and S2c), while the downward longwave radiation flux increased by up to 70 W m^{-2}. This was accompanied by a halving of the amplitude of the temperature diurnal cycle, driven mostly by an increase in the nighttime

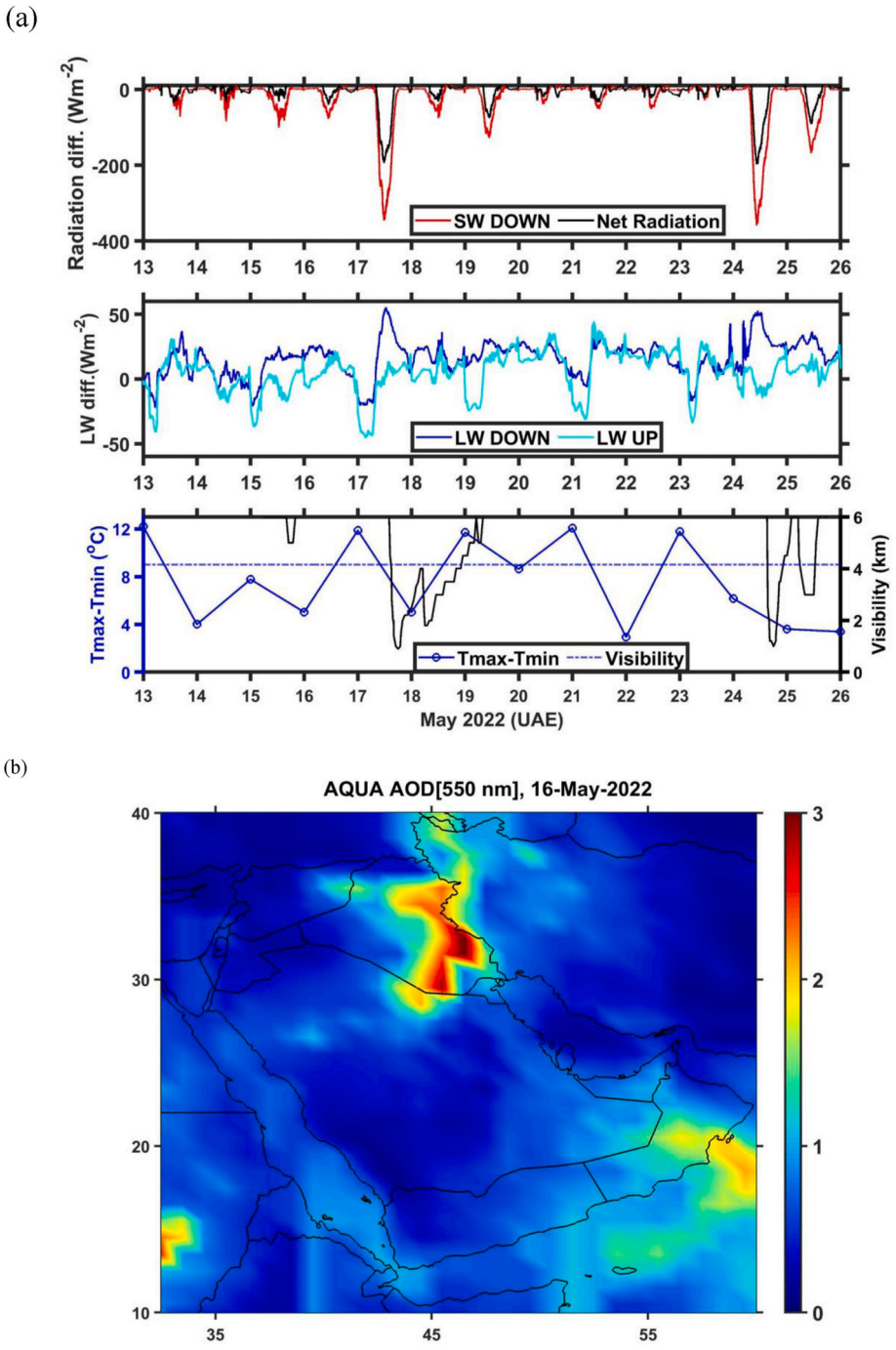

Fig. 7. Radiative impact of dust storms: (a) All-sky surface downwards (red and blue) and upwards (green and cyan) shortwave and longwave radiation fluxes (W m^{-2}) and net radiation flux (black; W m^{-2}) as measured by a radiation sensor at Barakah (asterisk in Fig. 1c) from May 13, 2022 at 00 LT to May 26, 2022 at 00 LT. The fluxes plotted are the anomalies with respect to the May 10, 2022 values, a clear/dust-free day. The third panel gives the amplitude of the air temperature diurnal cycle (°C) and horizontal visibility (km) at Barakah (asterisk in Fig. 1c) and Abu Dhabi (cross in Fig. 1c), respectively. The temporal resolution is 1 min for the radiation fluxes and 10 min for the weather fields. (b) AOD at 550 nm from the MODIS instrument on board the Aqua satellite on May 16, 2022. (c) Daily-averaged surface downward shortwave radiation flux (left; W m^{-2}) and longwave radiation flux (right; W m^{-2}) anomalies on May 16, 2022 from the Clouds and Earth's Radiant Energy System (CERES; Kratz et al., 2014; Kratz et al., 2020) data, available on a 1° × 1° grid, with respect to the 2000–2019 May climatology. The white pixels denote missing data. (d) Daily temperature anomalies (°C) at 12 UTC in the bottom 16 km of the atmosphere as measured by radiosondes launched at Abu Dhabi's Airport (cross in Fig. 1c) for May 2022. The anomalies are computed with respect to the 2009–2019 May climatology.

(c)

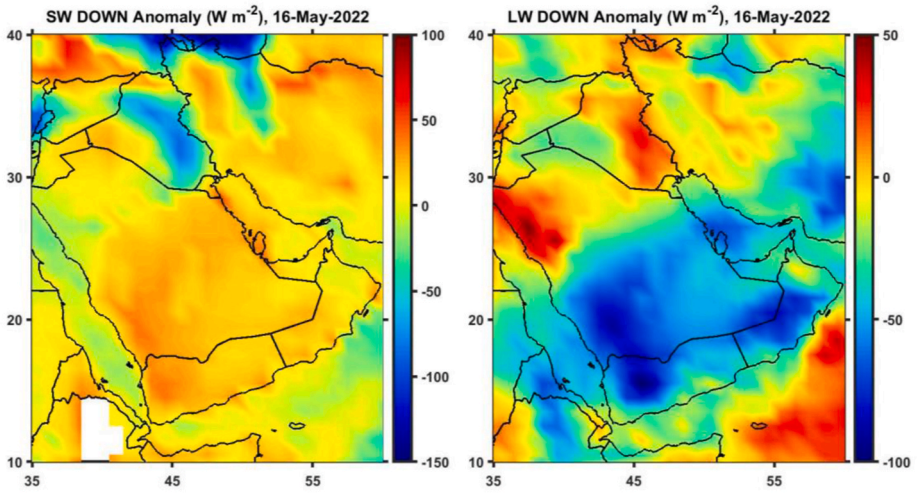

(d)

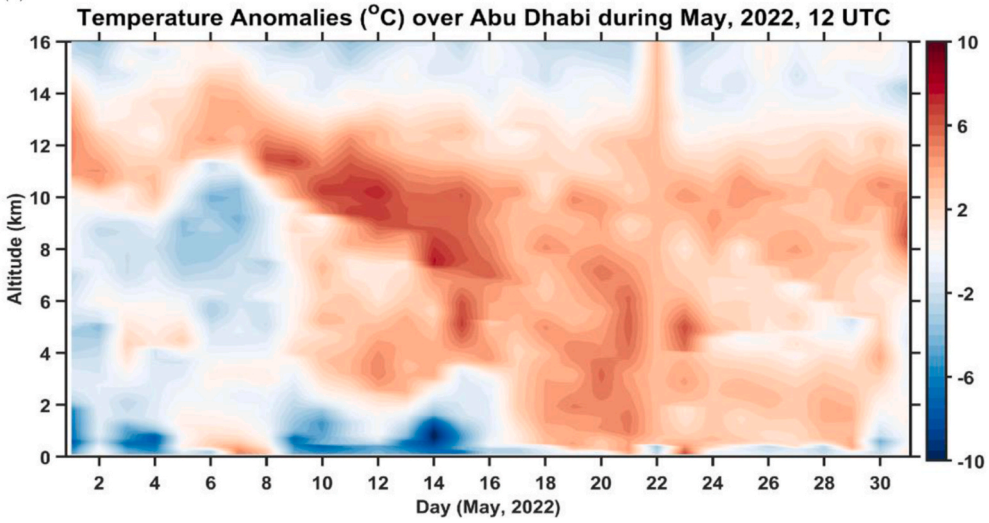

Fig. 7. (*continued*).

temperatures (Fig. S2b). While on 18 May the radiation fluxes went back to pre-event levels, the second event lasted longer, with the dust effects still present on 25 May. This is consistent with the higher AODs (Fig. 6a) and a prolonged duration of the second event: while in the first the AOD only exceeded 1 on 19 May, in the second it remained above 1 from 25–28 May (Fig. S2c). What is more, the observed AODs on 19 and 25 May are on the higher end of the May climatological distribution at Barakah (Fig. 6a), stressing the extreme nature of the May 2022 dust events. It is important to note that, in the May 2022 case, the bulk of the dust plumes was not over the site but to its north and west (Fig. 5b–e). Hence, a larger impact is expected for the core of the dust plumes located over Saudi Arabia and Kuwait. Not only were the May 2022 dust episodes remarkable in terms of magnitude, but they were also noteworthy regarding their duration: as shown in Fig. 6b, the duration of the 17 and May 24, 2022 dust events at a station near the emission site and at Abu Dhabi, located downstream, comprises the highest value for May 1983–2022 for Abu Dhabi and the second and third highest at Abadan in southwestern Iran. It is interesting to note that the duration of dust events at Abu Dhabi exhibits a pronounced decadal variability. This has been noted by Basha et al. (2019) and Aldababseh and Temimi (2017). The latter study found a strong positive and negative correlation between the number of yearly dust events at Abu Dhabi and the Pacific Decadal Oscillation and the Atlantic Multidecadal Oscillation, respectively. In southwestern Iran there is also considerable inter-annual to decadal variability in springtime dust events, largely controlled by changes in precipitation in association with shifts in the Mediterranean storm track (Yu et al., 2015).

The dust impacts can also be seen at night; on 17 May when the dust reached the UAE, a 70 W m^{-2} increase in the downward longwave radiative flux was registered during night and is due to the re-emission of LW radiation by the layer of atmospheric dust which was blanketing the country. Similar conditions were observed during night on 23–24 May where two sudden jumps in the downward longwave radiation flux of about 40 W m^{-2} were seen in the observations. The cooling effect of atmospheric dust in the near-surface layer during day and warming during night has been demonstrated to inhibit planetary boundary layer (PBL) development in daytime but has an opposite effect at night (Zhang et al., 2022). The same pattern is seen in Fig. 5f where the PBL height during the day was lower than during evening hours. Besides the effects of dust, the warm nighttime temperatures can be attributed to changes in wind speed/direction (warmer onshore vs. cooler offshore temperature advection) and moisture content (enhanced nighttime radiative warming in a moist atmosphere and vice-versa, Nelli et al., 2020).

Over the full domain, daily-mean surface fluxes derived from CERES satellite data are shown in Fig. 7 b-c and S4a-d. The radiative signatures of the dust, namely the reduction in the downward shortwave flux and

increase in the downward longwave flux, can be clearly seen. On 16 May over Iraq, where the bulk of the dust plume was located (Fig. 7b), the downward SW flux dropped by about 75 W m^{-2} and the upward LW flux jumped by about 40 W m^{-2}; 10–20% of the absolute values (Fig. S4a), as the dust clouds swept through. On 24 May (Fig. S4b-d), the majority of the dust was over the Arabian Gulf and eastern Saudi Arabia (Fig. S4b), with a comparable radiative effect (Figs. S4c-d).

The warming effect of the dust clouds throughout the atmospheric layer can also be seen in temperature profiles measured by radiosondes launched at Abu Dhabi's Airport (Fig. 7d) and in the columnar radiative effect estimated from the surface and top of the atmosphere radiation fluxes (Fig. S4e). During the first 10 days of May 2022, an anomalous warm layer (relative to the 2009–2019 May climatology) was present between 10 and 14 km, with the warm layer descending to the mid-troposphere on 10 May. This warming in the 10–14 km layer in early May corresponds to subsidence and associated adiabatic compression due to the presence of the subtropical high over the region (Fig. 2d). During the rest of the month, warmer than usual conditions (up to 6 °C above the climatological mean) dominated throughout the troposphere and were associated with the thick dust layers that succeeded over Abu Dhabi as confirmed by an inspection of the ceilometer data (not shown). The signature of the dust storms on the warming in the atmosphere was particularly pronounced after 18 May (Fig. 7d), i.e., after the first dust storm had reached Abu Dhabi.

6. Conclusions

In this work, a newly identified atmospheric trigger for dust emission in the spring season over the Middle East, namely atmospheric rivers from the tropics combined to cold drops from mid-latitudes and the associated convective-driven density currents, is presented. The large-scale circulation that promoted the occurrence of the cold-drops over the Middle East is also analyzed. Finally, the spatio-temporal characteristics of the May 2022 Middle East dust storms and their impact on the environment and the radiative budget are discussed based on a unique dataset acquired recently over southern Arabian Peninsula. A wave-number 5 pattern in the atmospheric circulation over the Northern Hemisphere conceived two deep troughs over north Africa and western Russia with a stationary ridge between them over Europe. This pattern in the circulation was characterized by a southward shift of the polar jet over the Mediterranean Sea leading to the occurrence of two cut-off lows over the eastern Mediterranean on 14–16 May and 21–23 May. Anomalous transport of tropical moisture in the form of atmospheric rivers was advected poleward around the cut-off lows as a result of the blocking over Saudi Arabia. These atmospheric rivers, combined with the diurnal heating, led to widespread convection over the mountainous regions in Turkey on 15–16 and 22–23 May. The associated downdrafts and density currents triggered dust emission at the surface, with the dust fronts propagating downstream towards the southern Arabian Peninsula. The dust storms were exceptional in their intensity, with the corresponding MODIS aerosol optical depths (AODs) in excess of 2.5, at the higher end of the climatological values observed during the last two decades over the region. Their duration was also remarkable, with a station adjacent to the emission region and another downstream reporting the second longest duration in the May climatological distribution, respectively. Cold drops from the mid-latitudes and atmospheric rivers from the tropics triggered the emission in the May 2022 dust episodes discussed here, a tropical-extratropical mechanism that has not been previously highlighted in the literature.

As a result of the dusty atmosphere, the daily maximum temperature in parts of Iraq dropped by more than 5 °C within a day, while in-situ observations in western United Arab Emirates showed a ~350 W m^{-2} drop in the downward shortwave radiation flux, or a third of its magnitude in a clear day, and a ~70 W m^{-2} increase in the downward longwave radiation flux. The nighttime temperature increased by roughly 9 °C and the amplitude of the temperature diurnal cycle dropped by a factor of two from 17 to 18 May. Satellite-derived estimates revealed a surface net radiative forcing of −20 W m^{-2}. The dust storms were associated with thick dust layers generating positive temperature anomalies (up to 6 °C) throughout the atmosphere with a pronounced warming at the dust layers' levels observed in the radiosonde profiles. This warming was also seen in the surface air temperature, especially during night, at individual sites in the region, and led to deeper boundary layers at night compared to daytime as estimated from lidar measurements.

Recent studies suggest dust storms are becoming more frequent in the Middle East (e.g. Al Ameri et al., 2019), with the recent droughts leading to new emission sources (Papi et al., 2022), and this trend can be amplified in a warmer world (e.g. Dai, 2011), with potentially disastrous consequences for human health (Soleimani et al., 2020). In fact, dust storms have major societal impacts ranging from health effects to disruptions to transportation, construction, education, energy and leisure activities (Beegum et al., 2018; Middleton et al., 2021). This study helps to increase our understanding on the mechanisms behind severe springtime dust storms in the region, noting the interaction between cold drops and atmospheric rivers as a new driver for dust emission. It also stresses the need to properly represent the large-scale atmospheric circulation in climate models, with higher-resolution simulations needed to capture the mesoscale processes that trigger dust emission. The direct observations of the dust radiative impacts presented here are unique in the region, and will help to reduce uncertainties in model simulations in a major dust source region.

Given the recent changes in the atmospheric circulation occurring over the northern hemisphere and their link to the Arctic amplification (e.g. Francis and Vavrus, 2012; Coumou et al., 2018), it is expected that the synoptic conditions identified here as triggers for severe dust storms over the Middle East can become more frequent under climate change. On the other hand, a recent study by Massoud et al. (2020) indicated that the frequency of atmospheric rivers is likely to increase in the Middle East and the Arabian Peninsula by the end of the century. Based on our findings and the link we found between a meandering polar jet, cut-off lows, atmospheric rivers and dust storms, there is a potential for the likelihood of the occurrence of the synoptic patterns identified here in a warming climate. Our findings pave the way for future projection studies to assess the tendency in dust storms over the Middle East in association with the identified atmospheric patterns.

CRediT authorship contribution statement

Diana Francis: Conceptualization, Validation, Writing – review & editing, Conception of the study, interpretation and validation of the results, review and revise the manuscript. **Ricardo Fonseca:** Writing – original draft, Formal analysis, Writing the original draft, revise the manuscript, data analysis and analysis of results. **Narendra Nelli:** Formal analysis, Data acquisition and analysis, data processing and inputs to the manuscript. **Deniz Bozkurt:** Formal analysis, and Data acquisition and analysis, data processing and inputs to the manuscript. **Juan Cuesta:** Formal analysis, Data acquisition and analysis, data processing and inputs to the manuscript. **Emmanuel Bosc:** Funding acquisition, Fund acquisition and inputs to the manuscript. All authors interpreted the results and provided input to the final manuscript.

Declaration of competing interest

The authors declare that they have no known competing financial interests or personal relationships that could have appeared to influence the work reported in this paper.

Data availability

Data will be made available on request.

Acknowledgements

We wish to acknowledge the contribution of Khalifa University's high-performance computing and research computing facilities and support team to the results of this research. We are also grateful to the Federal Authority for Nuclear Regulation (FANR; https://www.fanr.gov.ae/en) and the Nawah Energy Company (https://www.nawah.ae/) for their invaluable support and assistance in the deployment of the instruments at Barakah site. This research work was supported by FANR through the research project Modeling of Radionuclides Dispersion in the UAE Environment (MORAD). The AEROIASI product is supported by the Centre National des Etudes Spatiales (CNES) through the IASI project (Terre Océan Surface Continentale Atmosphère). We would like to thank the two anonymous reviewers for their several insightful comments/suggestions that helped to substantially improve the quality of the manuscript.

Appendix A. Supplementary data

Supplementary data to this article can be found online at https://doi.org/10.1016/j.atmosenv.2022.119539.

References

Al Ameri, I.D.S., Briant, R.M., Engels, S., 2019. Drought severity and increased dust storm frequency in the Middle East: a case study from the Tigris-Euphrates alluvian plain, central Iraq. Weather 74, 416–426. https://doi.org/10.1002/wea.3445.

Albrecht, B.A., 1989. Aerosols, cloud microphysics, and fractional cloudiness. Science 245, 1227–1230. https://doi.org/10.1126/science.245.4923.1227.

Aldababseh, A., Temimi, M., 2017. Analysis of the long-term variability of poor visibility events in the UAE and the link with climate dynamics. Atmosphere 8, 242. https://doi.org/10.3390/atmos8120242.

Allen, C.J.T., Washington, R., 2014. The low-level jet dust emission mechanism in the central Sahara: observations from the Bordj-Badji Mokhtar during the June 2011 fennec intensive observation period. J. Geophys. Res. Atmos. 119, 2990–3015. https://doi.org/10.1002/2013JD020594.

Banks, J.R., Hunerbein, A., Heinold, B., Brindley, H.E., Deneke, H., Schepanski, K., 2019. The sensitivity of the colour of dust in MSG-SEVIRI Desert Dust infrared composite imagery to surface and atmospheric conditions. Atmos. Chem. Phys. 19, 6893–6911. https://doi.org/10.5194/acp-19-6893-2019.

Basha, G., Ratnam, M.V., Niranjan Kumar, K., Ouarda, T.B.M.J., Kishore, P., Velicogna, I., 2019. Long-term variation of dust episodes over the United Arab Emirates. J. Atmos. Sol. Terr. Phys. 187, 33–39. https://doi.org/10.1016/j.jastp.2019.03.006.

Beegum, S.N., Gherboudj, I., Chaouch, N., Temimi, M., Ghedira, H., 2018. Simulation and analysis of synoptic scale dust storms over the Arabian Peninsula. Atmos. Res. 199, 62–81. https://doi.org/10.1016/j.atmosres.2017.09.003.

Behzad, H., Ohyanagi, H., Alharbi, B., Ibarra, M., Alarawi, M., Saito, Y., Duarte, C.M., Bajic, V., Mineta, K., Gojobori, T., 2022. A cautionary signal from the Red Sea on the impact of increased dust activity on marine microbiota. BMC Genom. 23, 277. https://doi.org/10.1186/s12864-022-08485-w.

Boller, R., 2022. National aeronautics and Space administration (NASA) Worldview. https://worldview.earthdata.nasa.gov/. (Accessed 18 May 2022).

Bou Karam, D., Flamant, C., Knippertz, P., Reitebuch, O., Pelon, J., Chong, M., Dabas, A., 2008. Dust emissions over the Sahel associated with the West African monsoon intertropical discontinuity region: a representative case-study. Q. J. R. Meteorol. Soc. 134, 621–634. https://doi.org/10.1002/qj.244.

Bou Karam, D., Williams, E., Janiga, M., Flamant, C., McGraw-Herdeg, M., Cuesta, J., Auby, A., Thorncroft, C., 2014. Synoptic-scale dust emissions over the Sahara Desert initiated by a moist convective cold pool in early August 2006. Q. J. R. Meteorol. Soc. 140, 2591–2607. https://doi.org/10.1002/qj.2326.

Bou Karam Francis, D., Flamant, C., Chaboureau, J.-P., Banks, J., Cuesta, J., Brindley, H., Oolman, L., 2017. Dust emission and transport over Iraq associated with the summer Shamal winds. Aeolian Research 24, 15–31. https://doi.org/10.1016/j.aeolia.2016.11.001.

Bozkurt, D., Sen, O.L., Ezber, Y., Guan, B., Viale, M., Caglar, F., 2021. Influence of African atmospheric rivers on precipitation and snowmelt in the near East's highlands. JGR-Atmospheres 126, e2020JD033646. https://doi.org/10.1029/2020JD033646.

Coumou, D., Di Capua, G., Vavrus, S., et al., 2018. The influence of Arctic amplification on mid-latitude summer circulation. Nat Commun 9, 2959. https://doi.org/10.1038/s41467-018-05256-8.

Cuesta, J., et al., 2008. Multiplatform observations of the seasonal evolution of the Saharan atmospheric boundary layer in Tamanrasset, Algeria, in the framework of the African Monsoon Multidisciplinary Analysis field campaign conducted in 2006. J. Geophys. Res. Atmos. 113, D00C07 https://doi.org/10.1029/2007JD009417.

Cuesta, J., Eremenko, M., Flamant, C., Dufour, G., Laurent, B., Bergametti, G., et al., 2015. Three-dimensional distribution of a major desert dust outbreak over East Asia in March 2008 derived from IASI satellite observations. J. Geophys. Res. Atmos. 120, 7099–7127. https://doi.org/10.1002/2014JD022406.

Cuesta, J., Flamant, C., Gaetani, M., Knippertz, P., Fink, A.H., Chazette, P., et al., 2020. Three-dimensional pathways of dust over the Sahara during summertime 2011 as revealed by new IASI observations. Q. J. R. Meteorol. Soc. 146, 2731–2755. https://doi.org/10.1002/qj.3814.

Dai, A., 2011. Drought under global warming: a review. WIREs Clim. Change 2, 45–65. https://doi.org/10.1002/wcc.81.

Dezfuli, A., Bosilovich, M.G., Barahona, D., 2021. A dusty atmospheric river brings floods to the Middle East. Geophys. Res. Lett. 48, e2021GL095441 https://doi.org/10.1029/2021GL095441.

Evan, A., Walkowiak, B., Frouin, R., 2022. On the misclassification of dust as cloud at an AERONET site in the sonoran desert. J. Atmos. Ocean. Technol. 39 (2), 181–191. https://doi.org/10.1175/JTECH-D-21-0114.1.

Fernald, F.G., 1984. Analysis of atmospheric lidar observations: some comments. Appl. Opt. 23, 652–653. https://doi.org/10.1364/AO.23.000652.

Filioglou, M., Giannakaki, E., Backman, J., Kesti, J., Hirsikko, A., Engelmann, R., O'Connor, E., Leskinen, J.T.T., Shang, X., Korhonen, H., Lihavainen, H., Romakkaniemi, S., Komppula, M., 2020. Optical and geometric aerosol particle properties over the United Arab Emirates. Atmos. Chem. Phys. 20, 8909–8922. https://doi.org/10.5194/acp-20-8909-2020.

Fonseca, R., Francis, D., Weston, M., Nelli, N., Farah, S., Wehbe, Y., AlHosari, T., Teixido, O., Mohamed, R., 2021. Sensitivity of summertime convection to aerosol loading and properties in the United Arab Emirates. Atmosphere 12 (12), 1687. https://doi.org/10.3390/atmos12121687.

Flamant, C., Chaboureau, J.-P., Parker, D.J., Taylor, C.M., Cammas, J.-P., Bock, O., Timouk, F., Pelon, J., Taylor, C., 2007. Airborne observations of the impact of a convective system on the planetary boundary layer thermodynamics and aerosol distribution in the inter-tropical discontinuity region of the West African Monsoon. Q. J. R. Meteorol. Soc. 133, 1175–1189.

Fonseca, R., Francis, D., Nelli, N., Thota, M., 2022. Climatology of the heat low and the intertropical discontinuity in the Arabian Peninsula. Int. J. Climatol. 42, 1092–1117. https://doi.org/10.1002/joc.7291.

Francis, D., Alshamsi, N., Cuesta, J., Isik, A.G., Dundar, C., 2019. Cyclogenesis and density currents in the Middle East and the associated dust activity in september 2015. Geosciences 9 (9), 376. https://doi.org/10.3390/geosciences9090376.

Francis, D., Fonseca, R., Nelli, N., Cuesta, J., Weston, M., Evan, A., Temimi, M., 2020a. The atmospheric drivers of the major Saharan dust storm in June 2020. Geophys. Res. Lett. 47, e2020GL090102 https://doi.org/10.1029/2020GL090102.

Francis, D., Mattingly, K.S., Temimi, M., Massom, R., Heil, P., 2020b. On the crucial role of atmospheric rivers in the two major Weddell Polynya events in 1973 and 2017 in Antarctica. Sci. Adv. 6, eabc2695. https://advances.sciencemag.org/content/6/46/eabc2695.

Francis, D., Chaboureau, J.-P., Nelli, N., Cuesta, J., Alshamsi, N., Temimi, M., Pauluis, O., Xue, L., 2021a. Summertime dust storms over the Arabian Peninsula and its impacts on radiation, circulation, cloud development and rain. Atmos. Res. 250, 105364 https://doi.org/10.1016/j.atmosres.2020.105364.

Francis, D., Temimi, M., Fonseca, R., Nelli, N.R., Abida, R., Weston, M., Wehbe, Y., 2021b. On the analysis of a summertime convective event in a hyperarid environment. Q. J. R. Meteorol. Soc. 147, 501–525. https://doi.org/10.1002/qj.3930.

Francis, D., Nelli, N., Fonseca, R., Weston, M., Flamant, C., Cherif, C., 2022a. The dust load and radiative impact associated with the June 2020 historical Saharan dust storm. Atmos. Environ. 268, 118808 https://doi.org/10.1016/j.atmosenv.2021.118808.

Francis, D., Fonseca, R., Nelli, N., Teixido, O., Mohamed, R., Perry, R., 2022b. Increased Shamal winds and dust activity over the Arabian Peninsula during the COVID-19 lockdown period in 2020. Aeolian Research 55, 100786. https://doi.org/10.1016/j.aerolia.2022.100786.

Francis, J.A., Vavrus, S.J., 2012. Evidence linking Arctic amplification to extreme weather in mid-latitudes. Geophys. Res. Lett. 39, 6.

Gandham, H., Dasari, H.P., Langodan, S., Karamuri, R.K., Hoteit, I., 2020. Major changes in extreme dust events dynamics over the Arabian Peninsula during 2003-2017 driven by atmospheric conditions. J. Geophys. Res. Atmos. 125, e2020JD032931 https://doi.org/10.1029/2020JD032931.

Griffiths, M., Reeder, M.J., Low, D.J., Vincent, R.A., 1998. Observations of a cut-off low over southern Australia. Q. J. R. Meteorol. Soc. 124, 1109–1132. https://doi.org/10.1002/qj.49712454805.

Gu, Y., Xue, Y., De Sales, F., Liou, K.N., 2016. A GCM investigation of dust aerosol impact on the regional climate of North Africa and South/East Asia. Clim. Dynam. 46, 2353–2370. https://doi.org/10.1007/s00382-015-2706-y.

Hameed, M., Ahmadalipour, A., Moradkhani, H., 2018. Apprehensive drought characteristics over Iraq: results of a multidecadal spatiotemporal assessment. Geosciences 8, 58. https://doi.org/10.3390/geosciences8020058.

Hamzeh, N.H., Karami, S., Kaskaoutis, D.G., Tegen, I., Moradi, M., Opp, C., 2021. Atmospheric dynamics and numerical simulations of six frontal dust storms in the Middle East region. Atmosphere 12, 125. https://doi.org/10.3390/atmos12010125.

Helgren, D.M., Prospero, J.M., 1987. Wind velocities associated with dust deflation events in the Western Sahara. J. Appl. Meteorol. Climatol. 26, 1147–1151. https://doi.org/10.1175/1520-0450(1987)026<1147:WVAWDD>2.0.CO;2.

Hersbach, H., Bell, B., Berrisford, P., Hirahara, S., Horanyi, A., Munoz-Sabater, J., Nicolas, J., Peavey, C., Radu, R., Schepers, D., Simmons, A., Soci, C., Abdalla, S., Abellan, X., Balsamo, G., Bachtold, P., Biavati, G., Bidlot, J., Bonavita, M., De Chiara, G., Dahlgren, P., Dee, D., Diamantakis, M., Dragani, R., Fleming, J., Forbes, R., Fuentes, M., Geer, A., Haimberger, L., Healy, S., Hogan, R.J., Holm, E., Janiskova, M., Keeley, S., Laloyaux, P., Lopez, P., Lupu, C., Radnoti, G., de

Rosnay, P., Rozum, I., Vamborg, F., illaume, S., Thepaut, J.-N., 2020. The ERA5 global reanalysis. Q. J. R. Meteorol. Soc. 146, 1999–2049. https://doi.org/10.1002/qj.3803.

Huang, J., Wang, T., Wang, W., Li, Z., Yan, H., 2014. Climate effects of dust aerosols over East Asia arid and semiarid regions. J. Geophys. Res. Atmos. 119, 11398–11416. https://doi.org/10.1002/2014JD021796.

Huang, J., Zhang, G., Zhang, Y., Guan, X., Wei, Y., Guo, R., 2020. Global desertification vulnerability to climate change and human activities. Land Degrad. Dev. 31, 1380–1391. https://doi.org/10.1002/ldr.3556.

IPCC, 2021. In: Masson-Delmotte, V., Zhai, P., Pirani, A., Connors, S.L., Pean, C., Berger, S., Caud, N., Chen, Y., Goldfarb, L., Gomis, M.I., Huang, M., Leitzell, K., Lonnoy, E., Matthews, J.B.R., Maycock, T.K., Waterfield, T., Yelekci, O., Yu, R., Zhou, B. (Eds.), Climate Change 2021: the Physical Science Basis. Cambridge University Press (in press). (Accessed 9 August 2021).

Jin, Y., Kai, K., Kewai, K., Nagai, T., Sakai, T., Yamazaki, A., Uchiyama, A., Batdorj, D., Sugimoto, N., Nishizawa, T., 2015. Ceilometer calibration for retrieval of aerosol optical properties. J. Quant. Spectrosc. Radiat. Transf. 153, 49–56. https://doi.org/10.1016/j.jqsrt.2014.10.009.

Johnson, B.T., Heese, B., McFarlane, S.A., Chazette, P., Jones, A., Bellouin, N., 2008. Vertical distribution and radiative effects of mineral dust and biomass burning aerosol over West Africa during DABEX. J. Geophys. Res. 113, D00C12. https://doi.org/10.1029/2008JD009848.

Kalenderski, S., Stenchikov, G., Zhao, C., 2013. Modeling a typical winter-time dust event over the arabian Peninsula and the Red Sea. Atmos. Chem. Phys. 13, 1999–2014. https://doi.org/10.5194/acp-13-1999-2013.

Kaskaoutis, D.G., Rashki, A., Houssos, E.E., Goto, D., Nastos, P.T., 2014. Extremely high aerosol loading over Arabian Sea during June 2008: the specific role of the atmospheric dynamics and Sistan dust storms. Atmos. Environ. 94, 374–384. https://doi.org/10.1016/j.atmosenv.2014.05.012.

Kaskaoutis, D.G., Dumka, U.C., Rashki, A., Psiloglou, B.E., Gavriil, A., Mofidi, A., Petrinoli, K., Karagiannis, D., Kambezidis, H.D., 2019a. Analysis of intense dust storms over the eastern Mediterranean in March 2018: impact on radiative forcing and Athens air quality. https://doi.org/10.1016/j.atmosenv.2019.04.025.

Kaskaoutis, D.G., Francis, D., Rashki, A., Chaboureau, J.-P., Dumka, U.C., 2019b. Atmospheric dynamics from synoptic to local scale during an intense frontal dust storm over the Sistan Basin in winter 2019. Geosciences 9, 453. https://doi.org/10.3390/geosciences9100453.

Kaufman, Y.J., Tanre, D., Rmer, L.A., Vermote, E.F., Chu, A., Holben, B.N., 1997. Operational remote sensing of tropospheric aerosol over land from EOS moderate resolution imaging spectroradiometer. J. Geophys. Res. 102, 17051–17067. https://doi.org/10.1029/96JD03988.

Kaufman, Y., Tanre, D., Boucher, O., 2002. A satellite view of aerosols in the climate system. Nature 419, 215–223. https://doi.org/10.1038/nature01091.

Kesti, J., Backman, J., O'Connor, E.J., Hirsikko, A., Asmi, E., Aurela, M., Makkonen, U., Filioglou, M., Komppula, M., Korhonen, H., Lihavainen, H., 2022. Aerosol particle characteristics measured in the United Arab Emirates and their response to mixing in the boundary layer. Atmos. Chem. Phys. 22, 481–503. https://doi.org/10.5194/acp-22-481-2022.

Kipp, Zonen, 2022. CNR4 net radiometer. available online at: https://www.kippzonen.com/Product/85/CNR4-Net-Radiometer. (Accessed 18 November 2022).

Knippertz, P., Deutscher, C., Kandler, K., Muller, T., Schulz, O., Schutz, L., 2007. Dust mobilization due to density currents in the Atlas region: observations from the Saharan Mineral Dust Experiment 2006 field campaign. J. Geophys. Res. 112, D21109 https://doi.org/10.1029/2007JD008774.

Kok, J.F., Abediyi, A., Albani, S., Balkanski, Y., Checa-Garcia, R., Chin, M., Colarco, P.R., Hamilton, D.S., Huang, Y., Ito, A., Klose, M., Li, L., Mahowald, N.M., Miller, R.L., Obiso, V., Garcia-Pando, C.P., Rocha-Lima, A., Wan, J.S., 2021. Contribution of the world's main dust source regions to the global cycle of desert dust. Atmos. Chem. Phys. 21, 8169–8193. https://doi.org/10.5194/acp-21-8169-2021.

Kratz, D.P., Stackhouse Jr., P.W., Gupta, S.K., Wilber, A.C., Sawaengphokhai, P., McGarragh, G.P., 2014. The fast longwave and shortwave flux (FLASHFlux) data product: single scanner footprint fluxes. J. Appl. Meteorol. Climatol. 53, 1059–1079. https://doi.org/10.1175/JAMC-D-13-061.1.

Kratz, D.P., Gupta, S.K., Wilber, A.C., Sothcott, V.E., 2020. Validation of the CERES edition-4A surface-only flux algorithms. J. Appl. Meteorol. Climatol. 59 (2), 281–295. https://doi.org/10.1175/JAMC-D-19-0068.1.

Leslie, J., Jones-Bateman, J., 2022. National Centers for environmental information (NCEI) national oceanic and atmospheric administration (NOAA). available online at: www.ncei.noaa.gov/. (Accessed 11 November 2022).

Li, Z., Li, C., Chen, H., Tsay, S.-C., Holben, B., Huang, J., Li, B., Maring, H., Qian, Y., Shi, G., Xia, X., Yin, Y., Zheng, Y., Zhuang, G., 2011. East Asian studies of tropospheric aerosols and their impact on regional climate (EAST-AIRC): an overview. J. Geophys. Res. 116, D00K34. https://doi.org/10.1029/2010JD015257.

Li, J., Carlson, B.E., Yung, Y.L., Lv, D., Hansen, J., Penner, J.E., Liao, H., Ramaswamy, V., Khan, R.A., Zhang, P., Dubovik, O., Ding, A., Lacis, A.A., Zhang, L., Dong, Y., 2022. Scattering and absorbing aerosols in the climate systems. Nat. Rev. Earth Environ. 3, 363–379. https://doi.org/10.1038/s43017-022-00296-7.

Lufft, 2022. WS501-UMB smart weather sensor. available online at: https://www.lufft.com/products/compact-weather-sensors-293/ws501-umb-smart-weather-sensor-1839/. (Accessed 18 November 2022).

Marcos, C.R., Gomez-Amo, J.L., Peris, C., Pedros, R., Utrillas, M.P., Martınez-Lozano, J. A., 2018. Analysis of four years of ceilometer-derived aerosol backscatter profiles in a coastal site of the western Mediterranean. Atmos. Res. 213, 331–345. https://doi.org/10.1016/j.atmosres.2018.06.016.

Martinez, M.A., Ruiz, J., Cuevas, E., 2009. Use of SEVIRI images and derived products in a WMO sand and dust storm warning system. IOP Conf. Ser. Earth Environ. Sci. 7, 012004 https://doi.org/10.1088/1755-1307/7/1/012004.

Massoud, E., Massoud, T., Guan, B., Sengupta, A., Espinoza, V., De Luna, M., Raymond, C., Waliser, D., 2020. Atmospheric rivers and precipitation in the Middle East and North Africa (MENA). Water 12, 2863. https://doi.org/10.3390/w12102863.

Mathbout, S., Lopez-Bustins, J.A., Martin-Vide, J., Bech, J., Rodrigo, F.S., 2018. Spatial and temporal analysis of drought variability at several time scales in Syria during 1961-2012. Atmos. Res. 200, 153–168. https://doi.org/10.1016/j.atmosres.2017.09.016.

Middleton, N.J., 2017. Desert dust hazards: a global review. Aeolian Research 24, 53–63. https://doi.org/10.1016/j.aeolia.2016.12.001.

Middleton, N., Kang, U., 2017. Sand and dust storms: impact mitigation. Sustainability 9, 1053. https://doi.org/10.3390/su9061053.

Middleton, N., Kashani, S.S., Attarchi, S., Rahnama, M., Mosalman, S.T., 2021. Synoptic causes and socio-economic consequences of a severe dust storm in the Middle East. Atmosphere 12, 1435. https://doi.org/10.3390/atmos12111435.

Miri, A., Ahmadi, H., Ekhtesasi, M.R., Panjehkeh, N., Ghanbari, A., 2009. Environmental and socio-economic impacts of dust storms in Sistan Region, Iran. Int. J. Environ. Stud. 66, 343–355. https://doi.org/10.1080/00207230902720170.

Mohammadpour, K., Sciortino, M., Saligheh, M., Raziei, T., Darvishi Boloorani, A., 2021. Spatiotemporal regionalization of atmospheric dust based on multivariate analysis of MACC model over Iran. Atmos. Res. 249, 105322 https://doi.org/10.1016/j.atmosres.2020.105322.

Mohammadpour, K., Rashki, A., Sciortino, M., Kaskaoutis, D.G., Darvishi Boloorani, A., 2022. A statistical approach for identification of dust-AOD hotspots climatology and clustering of dust regimes over Southwest Asia and the Arabian Sea. Atmos. Pollut. Res. 13, 101395 https://doi.org/10.1016/j.apr.2022.101395.

Munkel, C., Eresmaa, N., Rasanen, J., Karppinen, A., 2007. Retrieval of mixing height and dust concentration with lidar ceilometer. Boundary-Layer Meteorol. 124, 117–128. https://doi.org/10.1007/s10546-006-9103-3.

Namdari, S., Karimi, N., Sorooshian, A., Mohammadi, G., Sehatkashani, S., 2018. Impacts of climate and synoptic fluctuations on dust storm activity over the Middle East. Atmos. Environ. 173, 265–276. https://doi.org/10.1016/j.atmosenv.2017.11.016.

Nelli, N.R., Temimi, M., Fonseca, R.M., Weston, M.J., Thota, M.S., Valappil, V.K., Branch, O., Wizemann, H.-D., Wulfmeyer, V., Wehbe, Y., 2020. Micrometeorological measurements in an arid environment: diurnal characteristics and surface energy balance closure. Atmos. Res. 234, 104745 https://doi.org/10.1016/j.atmosres.2019.104745.

Nelli, N., Fissehaye, S., Francis, D., Fonseca, R., Temimi, M., Weston, M., Abida, R., Nesterov, A., 2021. Characteristics of atmospheric aerosols over the UAE inferred from CALIPSO and sun photometer aerosol optical depth. Earth Space Sci. 8, e2020EA001360 https://doi.org/10.1029/2020EA001360.

Nelli, N., Francis, D., Fonseca, R., Bosc, E., Addad, Y., Temimi, M., Abida, R., Weston, M., Cherif, C., 2022. Characterization of the atmospheric circulation near the Empty Quarter Desert during major weather events. Front. Environ. Sci. 10, 972380 https://doi.org/10.3389/fenvs.2022.972380.

Nieto, R., Gimeno, L., de la Torre, L., Ribera, P., Gallego, D., Garcia-Herrera, R., Garcia, J. A., Munez, M., Redano, A., Lorente, J., 2005. Climatological features of cutoff low systems in the northern hemisphere. J. Clim. 18, 3085–3103. https://doi.org/10.1185/JCLI13386.1.

Notaro, M., Alkolibi, F., Fadda, E., Bakhrjy, F., 2013. Trajectory analysis of Saudi Arabian dust storms. J. Geophys. Res. Atmos. 118, 6028–6043. https://doi.org/10.1002/jgrd.50346.

Oolman, L., 2022. University of Wyoming - atmospheric soundings (dataset). Accessed on 10 June 2022, data available online at. https://weather.uwyo.edu/upperair/sounding.html.

Papi, R., Attarchi, S., Boloorani, A.D., Samany, N.N., 2022. Characterization of hydrologic sand and dust storm sources in the Middle East. Sustainability 14, 15352. https://doi.org/10.3390/su142215352.

Parajuli, S.P., Stenchikov, G.L., Ukhov, A., Shevchenko, I., Dubovik, O., Lopatin, A., 2020. Aerosol vertical distribution and interactions with land/sea breezes over the eastern coast of the Red Sea from lidar data and high-resolution WRF-Chem simulations. Atmos. Chem. Phys. 20, 16089–16116. https://doi.org/10.5194/acp-20-16089-2020.

Porcu, F., Carrassi, A., Medaglia, C., Prodi, F., Mugnai, A., 2007. A study on cut-off low vertical structure and precipitation in the Mediterranean region. Meteorol. Atmos. Phys. 96, 121–140. https://doi.org/10.1007/s00703-006-0224-5.

Rashki, A., Kaskaoutis, D.G., Mofidi, A., Minvielle, F., Chiapello, I., Legrand, M., Dumka, U.C., Francois, P., 2019. Effects of monsoon, shamal and levar winds on dust accumulation over the Arabian Sea during summer - the july 2016 case. Aeolian Research 36, 27–44. https://doi.org/10.1016/j.aeolia.2018.11.002.

Reddy, N.N., Rao, K.G., 2018. Contrasting variations in the surface layer structure between the convective and non-convective periods in the summer monsoon season for Bangalore location during PRWONAM. J. Atmos. Sol. Terr. Phys. 167, 156–168. https://doi.org/10.1016/j.astp.2017.11.017.

Rezazadeh, M., Irannejad, P., Shao, Y., 2013. Climatology of the Middle East dust events. Aeolian Research 10, 103–109. https://doi.org/10.1016/j.aeolia.2013.04.001.

Rosenfeld, D., Woodley, W.L., Khain, A., Cotton, W.R., Carrio, G., Ginis, I., Golden, J.H., 2012. Aerosol effects on microstructure and intensity of tropical cyclones. Bull. Am. Meteorol. Soc. 93, 987–1001. https://doi.org/10.1175/BAMS-D-11-00147.1.

Salmabadi, H., Khalidy, R., Saeedi, M., 2020. Transport routes and potential source regions of the Middle Eastern dust over Avhaz during 2005-2017. Atmos. Res. 241, 104947 https://doi.org/10.1016/j.atmosres.2020.104947.

Schepanski, K., Tegen, I., Laurent, B., Heinold, B., Macke, A., 2007. A new Saharan dust source activation frequency map derived from MSG-SEVIRI IR-channels. Geophys. Res. Lett. 34, L18803 https://doi.org/10.1029/2007GL030168, 10.1029/2007GL030168.

Schmetz, J., Pili, P., Tjemkes, S., Just, D., Kerkmann, J., Rota, S., Ratier, A., 2002. An introduction to Meteosat second generation (MSG). Bull. Am. Meteorol. Soc. 83, 977–993. https://doi.org/10.1175/1520-0477(2002)083,0977:AITMSG.2.3.CO;2.

Singh, S., Beegum, S.N., 2013. Direct radiative effects of an unseasonable dust storm at a western Indo Gangetic Plain station in Delhi in ultraviolet, shortwave, and longwave regions. Geophys. Res. Lett. 40, 2444–2449. https://doi.org/10.1002/grl.50496.

Singh, A., Tiwari, S., Sharma, D., Singh, D., Tiwari, S., Srivastava, A.K., Rastogi, N., Singh, A.K., 2016. Characterization and radiative impact of dust aerosols over northwestern part of India: a case study during a severe dust storm. Meteorol. Atmos. Phys. 128, 779–792. https://doi.org/10.1007/s00703-016-0445-1.

Slingo, A., Ackerman, T.P., Allan, R.P., Kassianov, E.I., McFarlane, S.A., Robinson, G.J., Barnard, J.C., Miller, M.A., Harries, J.E., Russell, J.E., Dewitte, S., 2006. Observations of the impact of a major Saharan dust storm on the atmospheric radiation balance. Geophys. Res. Lett. 33, L24817 https://doi.org/10.1029/2006GL027869.

Soleimani, Z., Teymouri, P., Boloorani, A.D., Mesdaghinia, A., Middleton, N., Griffin, D. W., 2020. An overview of bioaerosol load and health impacts associated with dust storms: a focus on the Middle East. Atmos. Environ. 223, 117187 https://doi.org/10.1016/j.atmosenv.2019.117187.

Solomos, S., Kallos, G., Mavromatidis, E., Kushta, J., 2012. Density currents as a desert dust mobilization mechanism. Atmos. Chem. Phys. 12, 11199–11211. https://doi.org/10.5194/acp-12-11199-2012.

Solomos, S., Ansmann, A., Mamouri, R.-E., Binietoglou, I., Patlakas, P., Marinou, E., Amiridis, V., 2017. Remote sensing and modelling analysis of the extreme dust storm hitting the Middle East and eastern Mediterranean in September 2015. Atmos. Chem. Phys. 17, 4063–4079. https://doi.org/10.5194/acp-17-4063-2017.

Tanaka, T.Y., Kurosaki, Y., Chiba, M., Matsumura, T., Nagai, T., Yamazaki, A., Uchiyama, A., Tsunematsu, N., Kai, K., 2005. Possible transcontinental dust transport from North Africa to the Middle East to East Asia. Atmos. Environ. 39, 3901–3909. https://doi.org/10.1016/j.atmosenv.2005.03.034.

Todd, M.C., Bou Karam, D., Cavazos, C., Bouet, C., Heinold, B., Baldasano, J.M., Cautenet, G., Koren, I., Perez, C., Solmon, F., Tegen, I., Tulet, P., Washington, R., Zakey, A., 2008. Quantifying uncertainty in estimates of mineral dust flux: an intercomparison of model performance over the Bodélé Depression, northern Chad. J. Geophys. Res. 113, D24107 https://doi.org/10.1029/2008JD010476, 10.1029/2008JD010476.

Todd, M.C., Allen, C.J.T., Bart, M., Bechir, M., Bentefouet, J., Brooks, B.J., Cavazos-Guerra, C., Clovis, T., Deyane, S., Dieh, M., Engelstaedter, S., Flamant, C., Garcia-Carreras, L., Gandega, A., Gascoyne, M., Hobby, M., Kocha, C., Lavaysse, C., Marsham, J.H., Martins, J.V., McQuaid, J.B., Ngamini, J.B., Parker, D.J., Podvin, T., Rocha-Lima, A., Traore, S., Wang, Y., Washington, R., 2013. Meteorological and dust aerosol conditions over the western Saharan region observed at Fennec Supersite-2 during the intensive observation period in June 2011. J. Geophys. Res. Atmos. 118, 8426–8447. https://doi.org/10.1002/jgrd.50470.

Weston, M.J., Temimi, M., Nelli, N.R., Fonseca, R.M., Thota, M.S., Valappil, V.K., 2020. On the analysis of the low-level double temperature inversion over the United Arab Emirates: a case study during April 2019. Geosci. Rem. Sens. Lett. IEEE 346–350. https://doi.org/10.1109/LGRS.2020.2972597.

Weston, M.J., Francis, D., Nelli, N., Fonseca, R., Temimi, M., Addad, Y., 2022. The first characterization of fog microphysics in the United Arab Emirates, an arid region on the Arabian Peninsula. Earth Space Sci. 9, e2021EA002032 https://doi.org/10.1029/2021EA002032.

Wiegner, M., Coauthors, 2014. What is the benefit of ceilometers for aerosol remote sensing? An answer from EARLINET. Atmos. Meas. Tech. 7, 1979–1997. https://doi.org/10.5194/amt-7-1979-2014.

Wielicki, B.A., Barkstrom, B.R., Harrison, E.F., Lee III, R.B., Smith, G.L., Cooper, J.E., 1996. Clouds and the Earth's radiant energy system (CERES). An Earth observing system experiment. Bull. Am. Meteorol. Soc. 77, 853–868. https://doi.org/10.1175/15020-0477(1996)077<0853:CATERE>2.0.CO.

Yang, S., Preißler, J., Wiegner, M., von Lowis, S., Petersen, G.N., Parks, M.M., Finger, D. C., 2020. Monitoring dust events using Doppler lidar and ceilometer in Iceland. Atmosphere 11, 1294. https://doi.org/10.3390/atmos11121294.

Yu, Y., Notaro, M., Liu, Z., Wang, F., Alkolibi, F., Fadda, E., Bakhrjy, F., 2015. Climatic controls on the interannual to decadal variability in Saudi Arabian dust activity: toward the development of a seasonal dust prediction model. J. Geophys. Res. Atmos. 120, 1739–1758. https://doi.org/10.1002/2014JD022611.

Yu, Y., Notaro, M., Kalashnikova, O.V., Garay, M.J., 2016. Climatology of summer Shamal wind in the Middle East. J. Geophys. Res. Atmos. 121, 289–305. https://doi.org/10.1002/2015JD024063.

Zhang, X., Xu, X., Chen, H., Hu, X.-M., Gao, L., 2022. Dust-planetary boundary layer interactions amplified by entrainment and advections. Atmos. Res., 106359 https://doi.org/10.1016/j.atmosres.2022.106359. ISSN 0169-8095.

Zhao, T.L., Gong, S.L., Zhang, X.Y., McKendry, I.G., 2003. Modeled size-segregated wet and dry deposition budgets of soil dust aerosol during ACE-Asia 2001: implications for trans-Pacific transport. J. Geophys. Res. 108, 8665. https://doi.org/10.1029/2002JD003363. D23.

Zittis, G., Almazroui, M., Alpert, P., Ciais, P., Cramer, W., Dahdal, Y., Fnais, M., Francis, D., Hadjinicolaou, P., Howari, F., Jrrar, A., Kaskaoutis, D.G., Kulmala, M., Lazoglou, G., Mihalopoulos, N., Lin, X., Rudich, Y., Sciare, J., Stenchikov, G., Xoplaki, E., Lelieveld, J., 2022. Climate change and weather extremes in the Eastern Mediterranean and Middle East. Rev. Geophys. 60, e2021RG000762 https://doi.org/10.1029/2021RG000762.